Strong Magnetic Coupling and Single-Molecule-Magnet Behavior in Lanthanide-TEMPO Radical Chains

Gang Huang, Carole Daiguebonne, Guillaume Calvez, Yan Suffren, Olivier Guillou, Thierry Guizouarn, Boris Le Guennic, Olivier Cador, Kevin Bernot

Strong Magnetic Coupling and Single-Molecule Magnet Behavior in Lanthanide-TEMPO Radical Chains

*Gang Huang, Carole Daiguebonne, Guillaume Calvez, Yan Suffren, Olivier Guillou, Thierry Guizouarn, Boris Le Guennic, Olivier Cador and Kevin Bernot**

Univ Rennes, INSA Rennes, CNRS, ISCR (Institut des Sciences Chimiques de Rennes) –UMR 6226, F-35000 Rennes, France

KEYWORDS: Lanthanides, radicals, TEMPO, magnetic coupling, magnetic chains, magneto-luminescent correlations.

ABSTRACT

Rational design of molecular chains made of *4f* ions and substituted TEMPO radical is presented. Reaction of $Ln(hfac)_3.2H_2O$ and TEMPO-CN radical affords air and moisture-stable isostructural molecular chains of formula $[Ln(hfac)_3TEMPO\text{-}CN]_n$ for $Ln = Gd^{III}$ and Tb^{III} whereas zero-dimensional complexes of formula $[Dy(hfac)_3(TEMPO\text{-}CN)_2][Dy(hfac)_3(H_2O)_2]_2$ are obtained for $Ln = Dy^{III}$ ($hfac^-$ = hexafluoroacetylacetonate, TEMPO-CN = 4-Cyano-2,2,6,6-tetramethylpiperidine 1-Oxyl).

To the best of our knowledge the Gd derivative, **Gd-TEMPO-CN**, shows one of the strongest antiferromagnetic (AF) coupling for Gd-radical pairs ever reported with $J_{Gd\text{-}rad}/k_B = -21.18$ K, 14.72 cm^{-1} ($H = -J\, S_{rad}\, S_{Gd}$ spin Hamiltonian convention). The Tb^{III} derivative, **Tb-TEMPO-CN**, also shows strong Tb-radical AF coupling that has been rationalized using *ab initio* CASSCF approach ($J_{Tb\text{-}rad} = -23.02$ K; -16.7 cm^{-1}) and confirmed by luminescence measurements. **Tb-TEMPO-CN** shows remarkable properties for a Tb-radical based SMM ($U_{eff} = 69.3 \pm 1$ K; $\tau_0 = 1.3 \times 10^{-7}$ s) and two different relaxation processes triggered by interchain magnetic coupling.

Introduction

Organic radicals are among the most efficient building blocks for the design of molecular magnetic materials. They provide strong magnetic coupling with metallic ions[1-3] and in particular, they are very well suited to bind *4f* ions whose shielded magnetic orbitals are usually a drawback for their use in extended magnetically-coupled structures. Accordingly, a large amount of *4f*-magnetic compounds[4-8] based on organic radicals including Single Molecule Magnets (SMM) or Single-chain magnets (SCM) has been reported.[9-13] Recently, astonishing examples of giant coercivity[14] and strong exchange coupling[15] on *4f*-radical molecules have been reported.

TEMPO-based radicals (TEMPO = 2,2,6,6-tetramethylpiperidine 1-Oxyl) can be considered as a subclass of nitroxide-based radicals. They show remarkable solid-state magnetic properties[16] with long-range magnetic ordering observable at low temperatures,[17] that recall the first observation of purely organic ferromagnet on p-nitrophenyl nitronyl nitroxide in the early 90's.[18]

Additionally, most of them are temperature-, air- and moisture-stable that is a considerable advantage in the search for advanced magnetic devices. Despite these results TEMPO radicals have received considerably less attention than other radicals[9,19] to build coordination complexes.

Indeed, in the search of complexes showing strong Gd-radical magnetic interactions[20-35] nitroxide radicals other than TEMPO have been preferred with record exchange coupling J = -17.4K ($H = -JS_{Gd} \cdot S_{rad}$ convention) observed on **Gd-6bpyNO** (6bpyNO = 2,2-bipyridine-6-yl tert-butyl nitroxide).[36] It has been demonstrated that a magnetic field as high as 52 Tesla is necessary to decouple the Gd-radical pair, making **Gd-6bpyNO** the highest AF coupled molecule from Gd-nitroxide compounds. A small chemical variation on the radical ligand afforded **Gd-PhNO** (PhNO = *tert*-butyl phenyl nitroxide) for which the record interaction, ferromagnetic in this case (J = +9 K), has been observed.[2] SMM properties have been also targeted and *4f*-nitroxides complexes with interesting magnetic slow relaxation of the Tb^{III} derivative have been reported[37-41] highlighting that strong Tb-radical magnetic coupling is able to induce efficient SMM properties even on systems where Tb^{III} ions (oblate by nature)[42] are in quite distorted environment.

Such small attention dedicated to TEMPO-based radical is somewhat surprising. First, because their similarity with the above mentioned record-breaking nitroxides should be appealing to build strongly magnetically-coupled molecules. Second, because the spin localization on the NO group of the TEMPO[43] is larger than the one on nitronyl-nitroxides[44,45] that have been extensively used to build hybrid organic-inorganic magnetic materials.[9,19,46] The coordination of TEMPO radicals on paramagnetic ions might thus lead to molecular edifices with relevant magnetic properties.

Indeed, magnetic chains based on *3d* ions and 4-subsituted TEMPO radical have been reported and some of them show significant coupling between the *3d* ion and the nitroxide radical.[47,48] Similarly, a beautiful example of *2p-3d-4f* complexes have been reported with N_3TEMPO (N_3TEMPO = 4-azido-2,2,6,6-tetramethylpiperidine-1-oxyl) providing various complex topologies and magnetic behaviors.[49]

First report of purely *4f* ion coordination on TEMPO radicals has been made in 2014 using the genuine TEMPO radical.[50] The TEMPO-Ln-TEMPO complex showed strong antiferromagnetic superexchange across diamagnetic La^{III} and Y^{III} ions (-7.45 and -24.9 K, respectively), with the Gd^{III} derivative that presents both ferro (+4 K) and antiferromagnetic interaction (-6.45 K).[50] Interestingly, the Er^{III} derivative[51] (an ion much less used in molecular magnetism than Dy^{III} and Tb^{III})[52,53] shows an SMM behavior that has been rationalized via magneto-luminescent correlations.[54] However, the study of a mono-bounded Gd-TEMPO complex showed significantly poorer magnetic behavior, highlighting the versatility of the magnetic coupling sign and strength upon coordination.[55]

TEMPO radical can be substituted to provide a nice example of binuclear compounds showing strong *4f*-radical magnetic coupling but also SMM behavior for the Dy^{III} and Tb^{III} derivatives.[56] This opens the way to extended TEMPO-based structures by appropriate substitution of the para position of the TEMPO radical.

In this work, we have used the TEMPO-CN radical (TEMPO-CN = 4-Cyano-2,2,6,6-tetramethylpiperidine 1-Oxyl, Scheme 1) that is able to bind and magnetically couple a lanthanide ion via its NO group but also to give rise to an extended magnetic network[57] via its CN coordinating group. The Gd, Tb and Dy derivatives (namely **Gd-TEMPO-CN**,

Tb-TEMPO-CN and **Dy-TEMPO-CN**) are presented. The targeted molecular chain has been obtained for the Gd^{III} and Tb^{III} derivatives with record AF coupling for the former and strong SMM behavior for the latter.

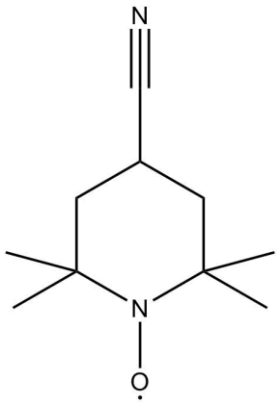

Scheme 1. Scheme of the TEMPO-CN radical (TEMPO-CN = 4-Cyano-2,2,6,6-tetramethylpiperidine 1-Oxyl).

EXPERIMENTAL SECTION

Starting materials: All starting reagents have been purchased from TCI chemicals and used without further purification.

Synthesis: $Ln(hfac)_3 \cdot 2H_2O$ precursors have been obtained via reported procedures ($hfac^-$ = hexafluoroacetylacetonate).[58] For **Dy-TEMPO-CN**, 0.1 mmol of $Dy(hfac)_3 \cdot 2H_2O$ have been dissolved in 15 mM n-heptane at 70°C and added to a 4 mL $CHCl_3$ solution containing 0.1 mmol of TEMPO-CN (TEMPO-CN = 4-Cyano-2,2,6,6-tetramethylpiperidine 1-Oxyl). The solution is stirred and filtered and pale prismatic yellow crystals obtained after several days. For **Tb-TEMPO-CN** and **Gd-TEMPO-CN** a similar procedure has been used and affords pale yellow needle-like crystals. Elemental Analysis Calculated (%) for $C_{65}H_{51}F_{54}N_4O_{24}Dy_3$: C,

27,97; H, 1.84; O, 13.76; found (%) C, 26.82; H, 1.81; O, 12.89. $C_{25}H_{20}F_{18}N_2O_7Tb_1$: C, 31.22; H, 2.10; O, 11.65; found (%) C, 31.16; H, 2.14; O, 11.69. $C_{25}H_{20}F_{18}N_2O_7Gd_1$: C, 31.25; H, 2.10; O, 11.66; found (%) C, 31.21; H, 2.13; O, 11.71. $C_{25}H_{20}F_{18}N_2O_7Eu_1$: C, 31.41; H, 2.11; O, 11.72; found (%) C, 31.32; H, 2.10; O, 11.72.

X-ray powder diffraction: Powder diffractograms have been obtained using a Panalytical X-Pert Pro diffractometer equipped with an X'celerator detector. Recording condition were 45 kV, 45 mA with Cu K_α ($\lambda = 1.542$ Å) in θ-θ mode. Simulated patterns from X-ray crystal structure have been obtained with Mercury 3.0 from CCDC.

Magnetic measurements: Magnetic measurements were performed on hand selected single-crystals crunched into powders and embedded in Teflon pellets in order to avoid micro-crystallite orientation under magnetic field. Magnetometer is a Quantum Design MPMS equipped with a low temperature ^{3}He probe for low temperature measurements ($0.5 < T < 2$ K). All measurements have been corrected from the contribution of the sample holder and from the diamagnetic contribution as calculated with Pascal's constants.

Luminescence measurements: Solid state emission and excitation spectra have been measured on a Horiba Jobin-Yvon Fluorolog III fluorescence spectrometer equipped with a Xe lamp 450 W, a UV-Vis photomultiplier (Hamamatsu R928, sensitivity 190 - 860 nm). Quantum yield measurements were performed using a Jobin-Yvon integrating sphere ($\Phi = (E_c-E_a)/(L_a-L_c)$ with E_c being the integrated emission spectrum of the sample, E_a the integrated "blank" emission spectrum, L_a the "blank" absorption and L_c the sample absorption at the excitation wavelength). The emission/excitation spectra and quantum yield recordings were realized on powder samples introduced in cylindrical quartz cells of 0.7 cm diameter and 2.4 cm height, which were placed

directly inside the integrating sphere. For the Tb(III) compound, single crystals were selected and mounted directly onto copper plates using conductive silver glue and cooled in an optical cryostat capable of reaching temperatures down to 77 K through a continuous nitrogen liquid flow and a nitrogen atmosphere inside the sample chamber (OptistatCF Oxford Inst.). Luminescence decays have also been measured using this apparatus with a Xenon flash lamp (phosphorescence mode). Lifetimes and quantum yields are averages of two independent determinations. Appropriate filters were used to remove the residual excitation laser light, the Rayleigh scattered light and associated harmonics from spectra. All spectra were corrected for the instrumental response function.

Crystal structure determination: Crystals have been mounted on a Bruker AXS diffractometer (APEXII) and crystal structures have been collected at 150 K with Mo K_α ($\lambda = 0.71073$ Å) radiation. Data reduction and cell refinement were performed with Denzo and Scalepack[59], crystal structures were solved by SIR97[60] and refined by SHELX97[61] via WINGX[62] interface. Hydrogens atoms were located to ideal positions. Squeeze procedure has been used to remove disordered solvent molecules. Crystal data can be found free of charge from Cambridge Crystallographic Data Center (wwww.ccdc.cam.ac.uk/data_request/cif) under reference (CCDC 1848211 (**Dy-TEMPO-CN**) and CCDC 1848892 (**Tb-TEMPO-CN**)

Computational details: CASSCF and SA-CASSCF/RASSI-SO calculations were carried out on the monomeric model complex of **Tb-TEMPO-CN** (see discussion section). The atomic positions of the molecule were extracted from the X-ray crystal structures and no geometry optimization was performed. All calculations were performed with the MOLCAS quantum chemistry package (versions 8.0).[63]

First, in order to compute the isotropic magnetic coupling between the Tb(III) ion and the radical ligand, CASSCF calculations were carried out without considering spin-orbit effects. The active space consisted in the seven *4f*-orbitals of the Tb(III) ion plus the singly-occupied antibonding π* orbital of the TEMPO-CN ligand: 9 electrons in 8 orbitals, CAS(9,8). Calculations were done on both the ferromagnetic and antiferromagnetic states obtained from the interaction of the unpaired electron of the TEMPO-CN radical and the unpaired electrons of the lanthanide ion. Thus the lowest octuplet and sextuplet were calculated. The value of the exchange coupling constant was computed within the Heisenberg model.

Second, the local electronic and magnetic properties on the Tb center were computed at the SA-CASSCF/RASSI-SO level by doping the TEMPO-CN radical with an extra electron to obtain a diamagnetic analogue. The active space only consists in 8 electrons in seven 4f-orbitals, i.e. CAS(8,7). In this approach, spin-orbit coupling was added within the restricted-active-space state-interaction (RASSI-SO) method, which uses the CASSCF spin-free wavefunctions as basis states.[64,65] State-averaged CASSCF calculations were performed for the seven septuplets and 140 quintuplets of the Tb(III) ion. All states were included in the RASSI-SO calculation. The resulting wavefunctions and energies are used to compute the magnetic properties and g-tensors of the lowest states from the energy spectrum by using the pseudospin S = 1/2 formalism in the SINGLE-ANISO routine.[66] This is made possible because despite being a non-Kramers ion, quasi-degenerate ground and first-excited spin-orbit states are found for Tb(III) (vide infra, Table S8). Simulations of $\chi_M T$ data were done with the POLY_ANISO program[67-69] using the computed single ion anisotropy. The exchange coupling interaction between the Tb center and the coordinated isotropic S = ½ radical was computed within the Lines model. Cholesky decomposition of the bielectronic integrals was employed to save disk space and speed-up the

calculations.[70] All atoms were described by ANO-RCC basis sets.[63,71,72] The following contractions were used: [8s7p4d3f2g1h] for Tb, [4s3p2d] for the O and N atoms, [3s2p] for C and F atoms and [2s] for the H atoms.

RESULTS AND DISCUSSION

Crystal structure description

The reaction of $Dy(hfac)_3 \cdot 2H_2O$ and TEMPO-CN radical affords compound **Dy-TEMPO-CN** that crystalizes in the *C2/c* space group (N°15). Main crystallographic data are reported in Table 1. The crystal structure can be described as one $Dy(hfac)_3$ entity (that involves Dy1 atom) coordinated by two different TEMPO-CN ligands through their NO groups that host the radical (Figure 1). Such coordination mode is likely to provide strong radical-Dy coupling. This molecule is surrounded by two uncoordinated $Dy(hfac)_3 \cdot 2H_2O$ molecules (that involve Dy2 atoms) that interact through H-bonds via one of their water molecules and the CN groups of the TEMPO-CN radicals. The second water molecule is involved in H-bonding with another $Dy(hfac)_3 \cdot 2H_2O$ molecule that further H-bonds another TEMPO-CN ligand (Figure 1, Figure S1). Overall the compounds can be considered as planes where radical-Dy-radical molecules alternate with chains of $Dy(hfac)_3 \cdot 2H_2O$ molecules. In these molecules Dy2-O_{hfac-} distances are in the range 2.302(4)-2.414(3) Å while for Dy1-O_{hfac-} the range is 2.336(3)-2.345(4). O4-Dy1-O4 angle is 141.14° and the two radical coordinated to Dy1 are almost parallel.

Numerous highly disordered solvent molecules have been found in between the planes and removed in the refinement process (Squeeze procedure). Dy1 is coordinated by six oxygen atoms from three $hfac^-$ anions and two nitroxide oxygen atoms from two radicals. Dy2 is coordinated by six oxygen atoms from three $hfac^-$ anions and two oxygen atoms from two water molecules.

Selected bond lengths and angles are listed in Table S1. The geometry of Dy1 coordination polyhedron is a triangular dodecahedron (D_{2d}, Continous Shape Measurement factor CSM = 0.431, Table S2)[73,74] whereas Dy2 can be described either by a distorted square antiprism (D_{4d}, CSM = 0.937) or a triangular dodecahedron (D_{2d}, CSM = 0.911). The smallest Dy-Dy distance is found between uncoordinated $Dy(hfac)_3$ molecules and the closest radical-Dy-radical molecule and is 6.06 Å.

Last, it is worth noticing that all attempts to force the uncoordinated $Dy(hfac)_3 \cdot 2H_2O$ entity to bind the CN group of the radical were unsuccessful (various heating procedures, reactant excess, …).

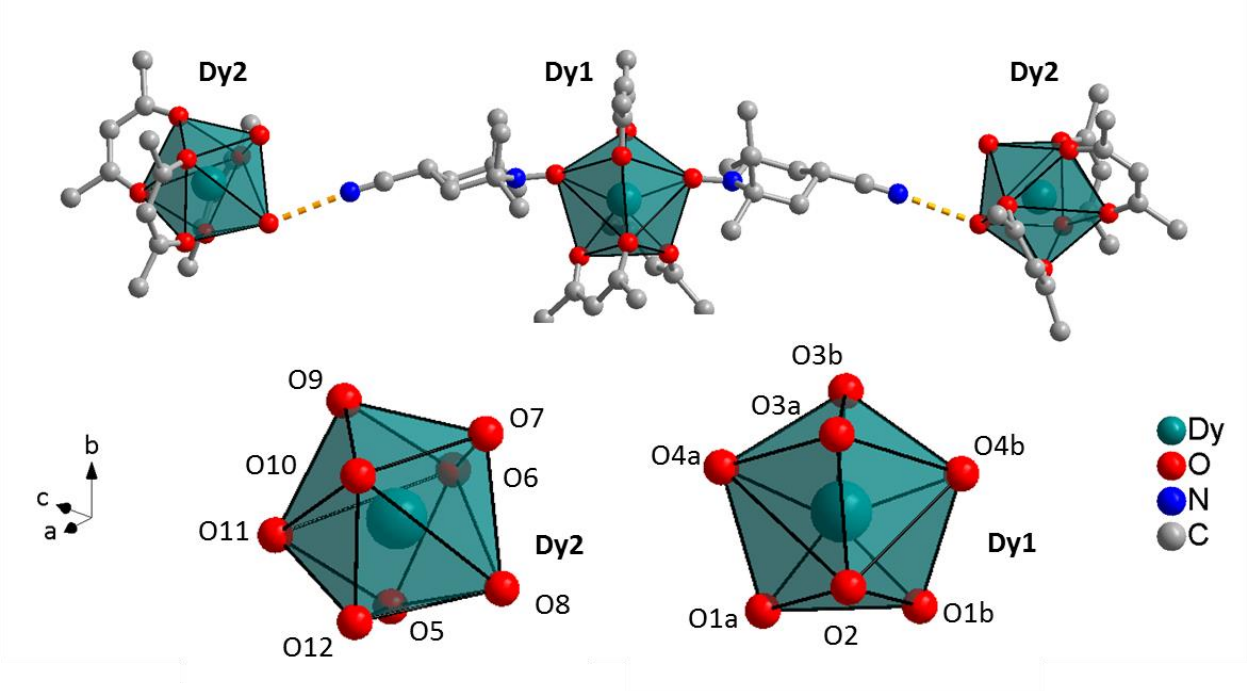

Figure 1. (top) Representation of **Dy-TEMPO-CN** and (bottom) coordination polyhedron of the two Dy^{III} ions. Hydrogen and fluorine atoms omitted for clarity.

The reaction of $Tb(hfac)_3 \cdot 2H_2O$ and TEMPO-CN radical (compound **Tb-TEMPO-CN)** affords single-crystal suitable of single-crystal X-ray diffraction. No single-crystals have been obtained for its Gd^{III} analogue, **Gd-TEMPO-CN,** but isostructurality is evidenced by powder X-ray diffraction (Figure S2). Compound **Tb-TEMPO-CN** crystallizes in the triclinic *P-1* space group (N°2). Main crystallographic data are reported in Table 1. The asymmetric unit is made of one $Tb(hfac)_3$ entity bounded to one TEMPO-CN molecule through its NO group from one side and another TEMPO-CN molecule through its CN group from the other side (Figure 2 and Figure 3). The N_{TEMPO}-Tb-O_{TEMPO} angle is 146.29° and the torsion angle of CN and NO group of a same TEMPO-CN is 170.40°. Overall a molecular chain is formed along the *b* axis. The Tb ion is in a O_7N_1 environment made of 6 oxygen atoms from three $hfac^-$ ancillary ligands, one oxygen from a NO group of a TEMPO-CN and one nitrogen from a CN group of another TEMPO-CN. The coordination environment is a distorted square antiprism (D_{4d}, CSM= 0.929, see Table S2).

The Tb-O_{hfac} bond lengths are in the 2.330(3)-2.387(3) Å range, while the Tb-O_{TEMPO} bond length is 2.2891(2) Å, slightly shorter than that of Tb-O_{hfac}. The Tb–N bond lengths are 2.540(3) Å. Additional bond lengths and angles are listed in Table S3. The shortest intrachain Tb-Tb distance is 11.12(6) Å, ruling out strong in-chain metal-metal and radical-radical interactions. The shortest interchain Tb–Tb distances are 8.41(5) Å, suggesting possible dipole-dipole interactions between the chains.

Table 1. Main crystallographic information for **Dy-TEMPO-CN** and **Tb-TEMPO-CN**.

Formula	$C_{65}H_{51}F_{54}N_4O_{24}Dy_3$ $[Dy(hfac)_3(TEMPO\text{-}CN)_2][Dy(hfac)_3(H_2O)_2]_2$ **(Dy-TEMPO-CN)**	$C_{25}H_{20}F_{18}N_2O_7Tb$ $[Tb(hfac)_3TEMPO\text{-}CN]_n$ **(Tb-TEMPO-CN)**
M[g.mol^{-1}]	2785.6	961.36

Crystal system	monoclinic	triclinic
Space group	*C2/c*	*P-1*
a(Å)	41.918(5)	11.0977(6)
b(Å)	11.197(5)	11.1157(5)
c(Å)	23.938(5)	16.4993(7)
α[°]	90	77.671(2)
β[°]	113.924(5)	74.378(2)
γ[°]	90	61.352(2)
V[Å^3]	10270(5)	1711.59(14)
Z	4	2
T(K)	150	150
2θ range	2.63-27.53	2.89-27.51
Reflns collected	23011	9967
Independent reflns	11821	7776
Observed reflns	11153	7134
Parameters	689	506
$R1/\omega R^2$	0.0385/0.1313	0.0341/0.0794
Goof	1.098	1.067

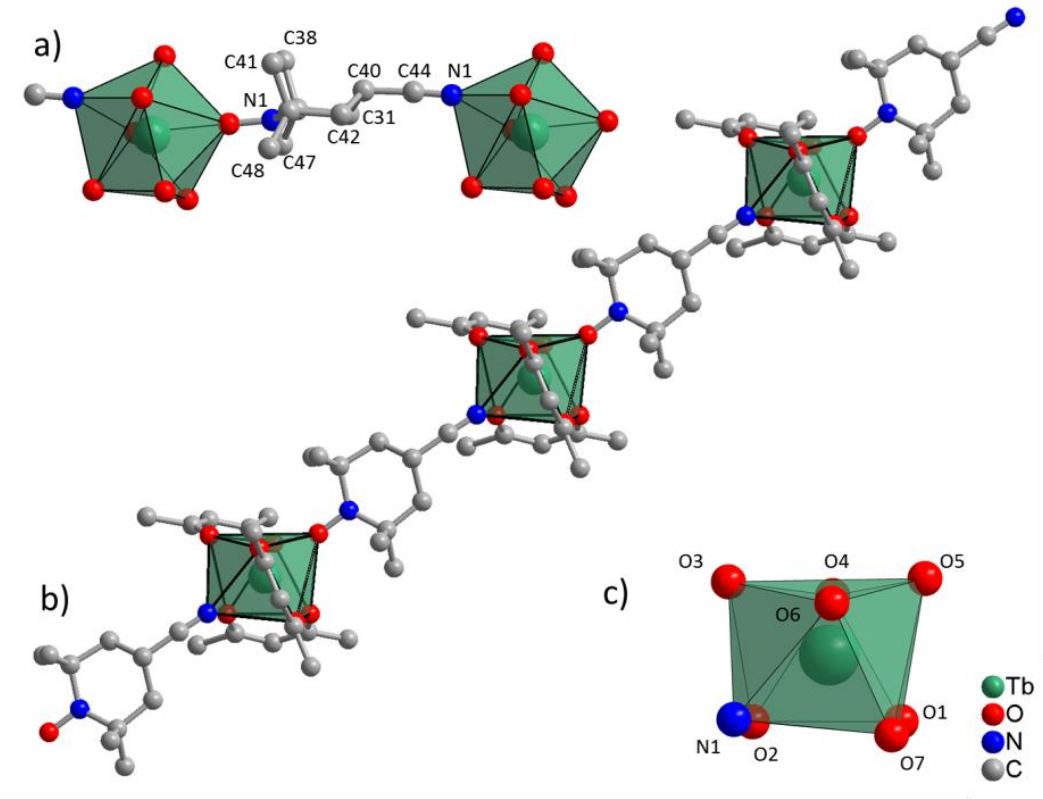

Figure 2. Representation of **Tb-TEMPO-CN** (hydrogen and fluorine atoms omitted for clarity). a) Label scheme of the TEMPO-CN ligand, b) representation of the chain structure, c) label scheme and coordination polyhedron of the Tb^{III} ion.

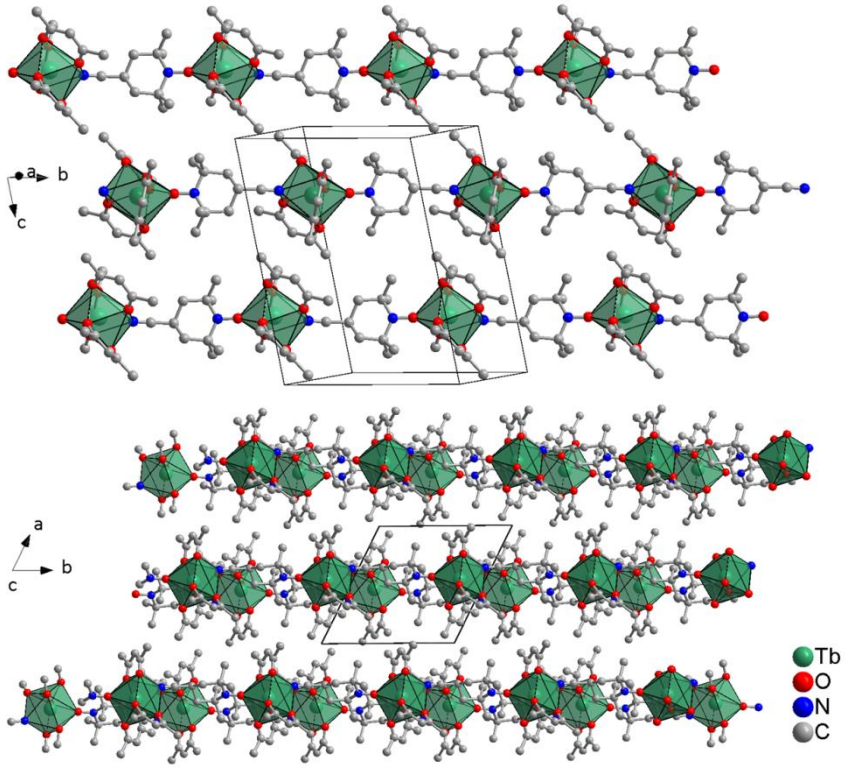

Figure 3. Representation of the crystal packing of **Tb-TEMPO-CN** close to the *bc* plane (top) and in the *ab* plane (bottom). Hydrogen and fluorine atoms omitted for clarity.

One can note that it has not been possible to obtain an isostructural compound made of Gd^{III} ion for this derivative. For a given lanthanide the crystallization of one crystal structure or the other maybe driven by the ionic radius of the Ln^{III} as commonly observed.[75]

Static magnetic properties

In order to quantify the magnetic coupling abilities of the TEMPO-CN radical with *4f* ions we have investigated first the Gd^{III} derivative, $[Gd(hfac)_3TEMPO\text{-}CN)]_n$ (**Gd-TEMPO-CN**), that is isostructural to **Tb-TEMPO-CN**. The room temperature $\chi_M T$ value is 8.38 $cm^3.K.mol^{-1}$ (Figure 4), close to the theoretical value expected for an uncoupled Gd^{III} ion ($^8F_{7/2}$, g = 2, $\chi_M T$ = 7.88 $cm^3.K.mol^{-1}$) plus one radical spin ($\chi_M T$ = 0.375 $cm^3.K.mol^{-1}$). Upon

cooling, the $\chi_M T$ value decreases progressively to reach a plateau around 15 K for $\chi_M T$ = 6.06 $cm^3.K.mol^{-1}$. This is a clear signature of a system that reaches $S_{total} = 3$. A final drop until 5.5 $cm^3.K.mol^{-1}$ at 2 K is attributed to weak intermolecular (interchain) antiferromagnetic couplings.[50] This behavior has been fitted considering the spin Hamiltonian $H = -J\, S_{rad}\, S_{Gd}$ with the introduction of a mean field zJ' intermolecular interaction (eq.1).

$$\chi_M T = \frac{4N_A g^2 \mu_B{}^2}{k_B} \frac{7 + 15\exp(4J_{Gd-rad}/k_B T)}{7 + 9\exp(4J_{Gd-rad}/k_B T)} \frac{T}{T - zJ'} \qquad \text{eq. (1)}$$

Best fit is obtained for $J_{Gd\text{-}rad}/k_B = -21.18 \pm 0.24$ K (-14.72 cm^{-1}), g = 2.01 ± 0.001, zJ' = -0.029 ± 0.001 K and $R^2 = 0.99804$. To the best of our knowledge this value is among the highest Gd-radical couplings ever reported and is overcome only by two reports on N_2^{3-} radical bridged dimers.[15,76] Indeed coupling constants on Gd-nitronyl-nitroxide radicals[9] or Gd-nitroxide radicals (see Scheme 2 and Table 2) are usually below a dozen of Kelvin.[9,31,56,77] The additional antiferromagnetic interchain interaction zJ' is found rather weak which is a common observation of dipolar interchain coupling in *4f*-radical-based chains.[78-80] The field dependence of magnetization at 2 K is depicted in the inset of Figure 4 and magnetization saturates at 6.06 μ_B close to the value expected for a $S_{total} = 3$ and g = 2 that confirms the strong AF coupling. Indeed the curve is almost superimposable with a simulation using Brillouin function for S = 3 at 2 K.[81]

On a theoretical point of view, DFT approaches demonstrated that the magnetic coupling mechanism is based on the overlap between the Gd^{III} magnetic orbitals and π* orbitals of the radical, these latter being able to gain occupation from the 5d/6s/6p Gd^{III} empty orbitals via charge transfer mechanism.[82] In this framework, the influence of Gd-O bond distance and/or on Gd-X-Y-C_{sp2} dihedral angles (where X-Y stands for O-N, O-C, N-C or N- N atoms)[2] has been considered. Actually, these two parameters have been used empirically to establish magneto-

structural correlations on Gd-nitroxide radical derivatives.[2,36,39,83] However, aforementioned DFT studies conclude that if each of these parameters is found relevant, no clear trend considering their mixed contribution over large series of compounds has been found.[82] We obtained a similar conclusion here on Gd-nitroxide compounds reported in Table 2.

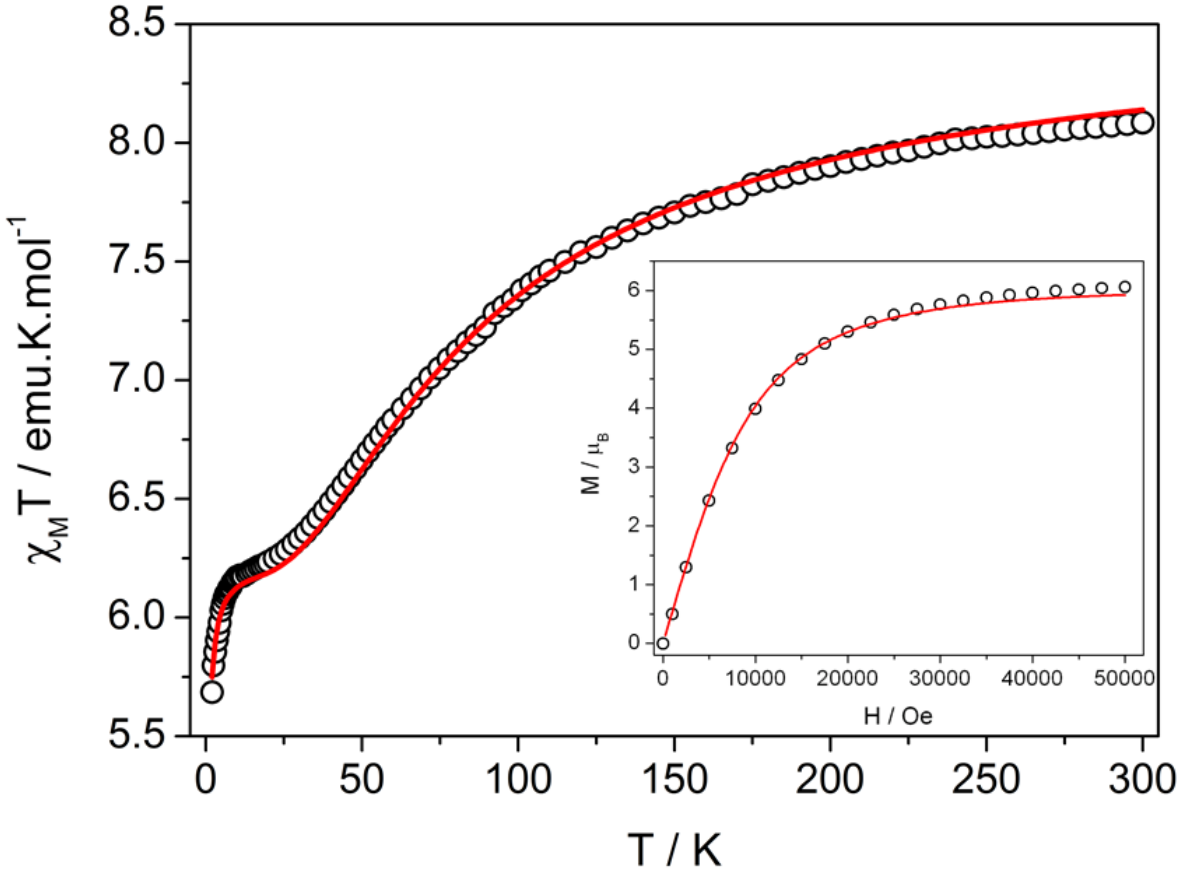

Figure 4. Temperature dependence of the $\chi_M T$ product for **Gd-TEMPO-CN** with the best fit obtained with equation 1 ($J_{Gd\text{-}rad}/k_B$ = -21.18 ± 0.24 K (-14.72 cm^{-1}), g = 2.01 ± 0.001, zJ' = -0.029 ± 0.001). The inset shows the field variation of the magnetization at 2 K with simulation of Brillouin function for S_{total} = 3.

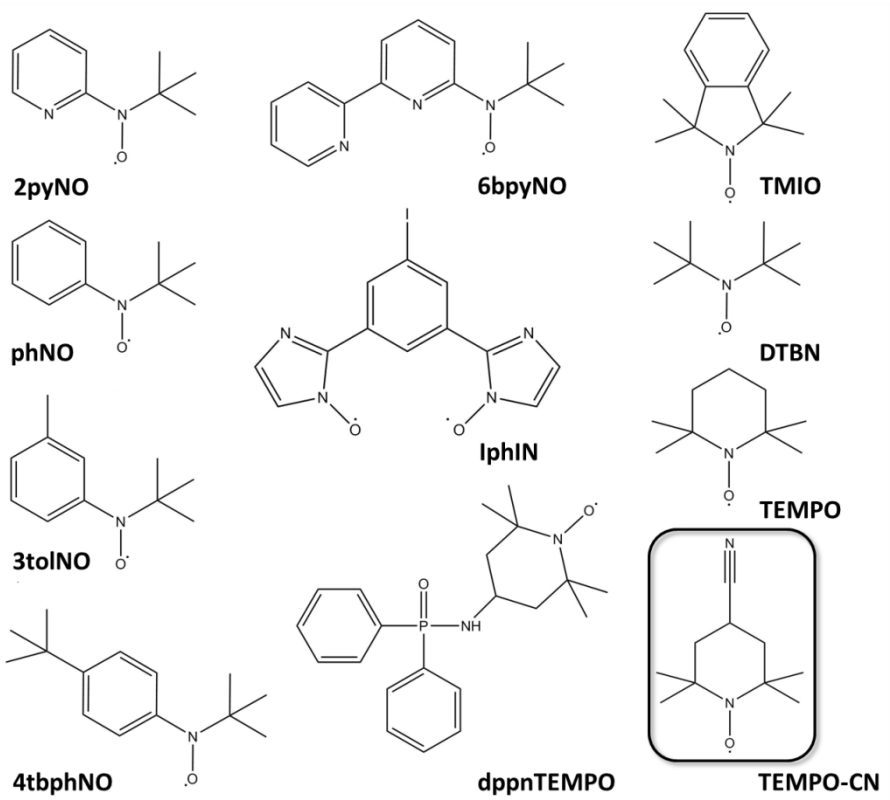

Scheme2: Nitroxide radical ligands used to design Gd^{III} or Tb^{III} nitroxide-based complexes (see Table 2 for coupling values and abbreviations).

Table 2: Magnetic coupling constants (K) observed on Gd^{III} or Tb^{III} nitroxide-based complexes (extension to other type of radicals available in ref [9]).

Compound	$J_{rad\text{-}Ln}$ (K)	Ref
Gd^{III}-based compounds		
$Gd(hfac)_3(2PyNO)(H_2O)$	-6.9	[31]
$Gd(hfac)_3(DTBN)(H_2O)$	-5.8	[84]
$Gd(hfac)_3(6bpyNO)$	-15.9 revised to -17.4	[36,83]
$Gd(hfac)_3(phNO)$	+9	[2]
$Gd(hfac)_3(3tolNO)$	8.35	[2]
$Gd(hfac)_3(4tbNO)$	3.75	[2]

$Gd(hfac)_3(TMIO)_2$	-6.3 ($J_{rad\text{-}rad}$ = -13.5)	[3]
Gd(hfac)3(MeOH)(TEMPO)	-1.8	[55]
$Gd_2(hfac)_6(H_2O)_2$(dppnTEMPO)	3.9	[56]
$[Gd_2(hfac)_6(IPhIN)(H_2O)_2]$	0.4 ($J_{rad\text{-}rad}$ = 9.4)	[85]
$[Gd(hfac)_3(IPhIN)(H_2O)]$	2 ($J_{rad\text{-}rad}$ = -5.6)	[85]
$Gd(hfac)_3(TEMPO)_2$	-6.5 / +4 ($J_{rad\text{-}rad}$ = 24.9)	[50]
$Gd_2(hfac)_6(H_2O)_2$(dppnTEMPO)	3.88 (zJ' = -0.028)	[56]
Gd-TEMPO-CN	-21.18 (zJ' = -0.029)	This work
Tb^{III}-based compounds		
$Tb_2(hfac)_6(H_2O)_2$(dppnTEMPO)	16.4	[56]
$Tb(hfac)_3$(2pyNO)	-9.57/-7.14	[39]
$Tb(hfac)_3(TMIO)_2$	-4.47	[41]
$Tb(hfac)_3$(6bpyNO)	ferro	[38]
Tb-TEMPO-CN	-23.02 K	This work

Abbreviations: 2PyNO = *tert*-butyl 2-pyridyl nitroxide, DTBN = di-t-butylnitroxide, 6bpyNO = 2,2-bipyridine-6-yl *tert*-butyl nitroxide, phNO = *tert*-butyl phenyl nitroxide, 3tolNO = N-*tert*-butyl-N-(3-tolyl)hydroxylamine), 4tbNO = N-*tert*-butyl-N-(4-*tert*-butylphenyl)hydroxylamine, TMIO = 1,1,3,3-tetramethylisoindolin-2-oxyl, dppn = (diphenylphosphinyl)amino, IPhIN = 1-iodo-3,5-bis(4',4',5',5'-tetramethyl-4',5'-dihydro-1H-imidazole-1'-oxyl)benzene), TEMPO = 2,2,6,6-tetramethylpiperidine 1-Oxyl.

Derivatives likely to give rise to SMM behavior[86] (**Dy-TEMPO-CN** and **Tb-TEMPO-CN**) have been also investigated by static magnetic measurements carried out on polycrystalline powders. On **Dy-TEMPO-CN**, the room temperature $\chi_M T$ value is 43.59 $cm^3.K.mol^{-1}$ in agreement with the expected value of 43.26 $cm^3.K.mol^{-1}$ for three isolated Dy^{III} ions ($^6H_{15/2}$, g = 4/3, $\chi_M T_{300K}$ = 14.17 $cm^3.K.mol^{-1}$) plus two radicals spins ($\chi_M T_{300K}$ = 0.75 $cm^3.K.mol^{-1}$) (Figure S3). Upon cooling, the $\chi_M T$ value decreases to reach 26.03 $cm^3.K.mol^{-1}$ at 2.0 K. This behavior is interplay between the depopulation of the Stark sub-levels of each of the Dy^{III} ions (Dy1 and Dy2) and possible Dy2-Dy2 and radical-Dy1 interactions. These numerous pathways for magnetic interactions make the evaluation of the radical-Dy1 interaction hardly reliable.

On **Tb-TEMPO-CN**, the room temperature $\chi_M T$ value is 11.98 $cm^3.K.mol^{-1}$ close to the expected value of 12.20 $cm^3.K.mol^{-1}$ for an uncoupled Tb^{III} ion ($^7F_6$, g = 3/2, $\chi_M T_{300K}$ = 11.82 $cm^3.K.mol^{-1}$) plus one radical spin ($\chi_M T_{300K}$ = 0.375 $cm^3.K.mol^{-1}$). Upon cooling, the $\chi_M T$ value decreases progressively to reach a plateau clearly visible at 5 K followed by a decrease towards 7.29 $cm^3.K.mol^{-1}$ at 2 K. A slight kink around 6 K is clearly visible (Figure 5). This lets suspect a dual contribution of the depopulation of Stark sub-levels of the Tb^{III} ion and an antiferromagnetic (AF) coupling in the Tb-radical pair. At low temperature (T < 5 K) the additional contribution of AF inter-chain interactions is also suspected.

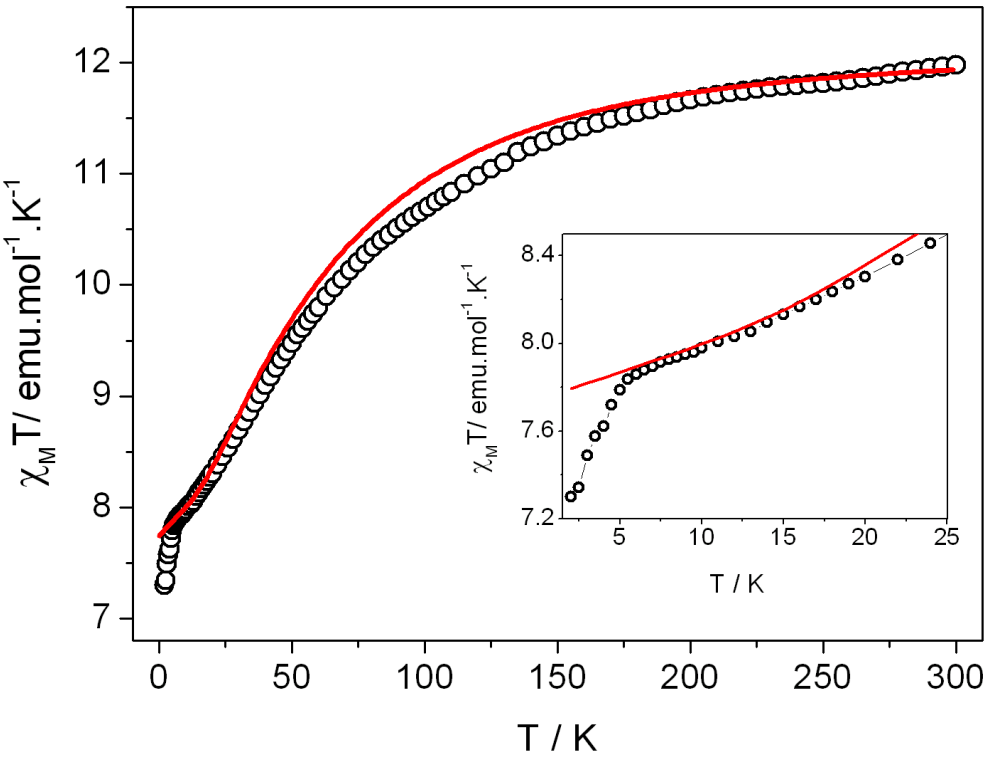

Figure 5. Temperature dependence of the $\chi_M T$ product for **Tb-TEMPO-CN** with low temperature region magnified in inset. Ab-initio simulation as red curve (see main text).

Ab-initio calculations

To get insights into the magnetic properties of **Tb-TEMPO-CN**, a two-step computational protocol based on CASSCF calculations was followed (see Computational details). This approach was used previously by Totti and coworkers on other series of lanthanide-radical complexes.[56,85,87] On one hand, SA-CASSCF/RASSI-SO calculations on the model complex (see Figure 6) with an extra electron on the TEMPO-CN radical have been performed. The computed energies of the low-lying electronic states are given in Table S8 and evidence both the quasi-degenerate ground spin-orbit state (0.17 cm^{-1}) and an overall splitting of the $^7F_6$ level of

501 cm^{-1}, in agreement with luminescence data (see below). Strong local easy-axis has been calculated for Tb (g_x = 0.000; g_y = 0.000; g_z = 17.74). As shown in Figure 6, the easy axis is orientated almost parallel to the square faces of the coordination polyhedron. On the other hand, CAS(9,8)SCF calculations with no spin-orbit contribution were carried out on the lowest octuplet and sextuplet states. Within the Heisenberg model, an antiferromagnetic $J_{(Tb\text{-}rad)}$ coupling of -23.02 K (-16.7 cm^{-1}) was computed. Based on these calculations the $\chi_M T$ vs. T curve was simulated with a great agreement with the experimental data (Figure 5 and Figure S4). No interchain interactions were considered in the simulations, explaining that the drop at low temperature is not reproduced.

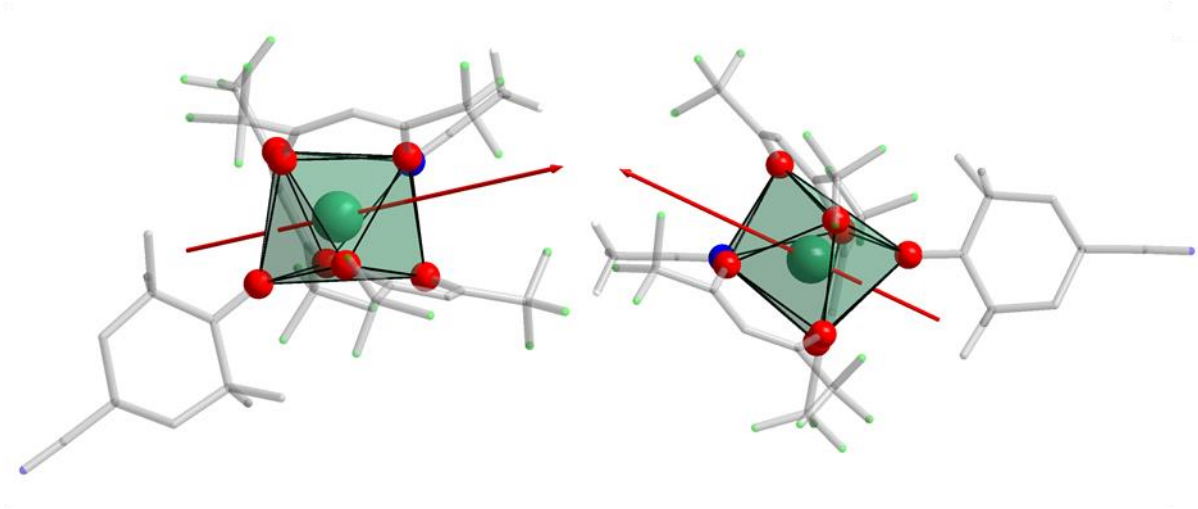

Figure 6. Representation (2 orientations are given) of the calculated fragment of **Tb-TEMPO-CN** with easy magnetization axis in red (hydrogen atoms omitted for clarity).

Magneto-luminescent correlations

Lanthanide ions can present luminescence in the visible region upon UV irradiation.[88] Some of us demonstrated that the detailed investigation of solid state luminescent spectrum of Ln-based SMMs is able to provide information on the energy scheme responsible for their magnetic

behavior.[54,89] This has also been generalized for NIR emissive Ln-SMM.[53,90-93] Since then magneto-luminescent correlations flourished.[94]

Low temperature (77 K) solid state luminescence spectra measured on a single-crystal of **Tb-TEMPO-CN** are provided in Figure 7. The excitation spectrum highlights a broad band below 330 nm that is attributed to $\pi^*(\text{hfac}) \rightarrow \pi(\text{hfac})$ transitions.[95] Hence, with $\lambda_{exc} = 325$ nm the characteristic Tb^{III} emission from $^5D_4 \rightarrow {}^7F_J$ radiative transitions is observed. Detailed measurement of the $^5D_4 \rightarrow {}^7F_6$ transition is provided in Figure 7 (see also Figures S5-S6). The overall splitting of the $^7F_6$ level is estimated to be 510 cm^{-1} that well matches with ab-initio calculations (501 cm^{-1}). Further deconvolution and analysis of this emission peak has not been possible because of the low emissive properties of **Tb-TEMPO-CN**. Accordingly, no reliable quantum yield and lifetime measurement could be extracted. No emission has been observed on **Dy-TEMPO-CN**. For information we provide the luminescence measurements of the **Eu-TEMPO-CN** in Figures S7. A quantum yield of $\varphi_{Lig\text{-}Eu} = 1.1(1)\%$ associated with a lifetime of $\tau = 0.43(1)$ ms is observed.

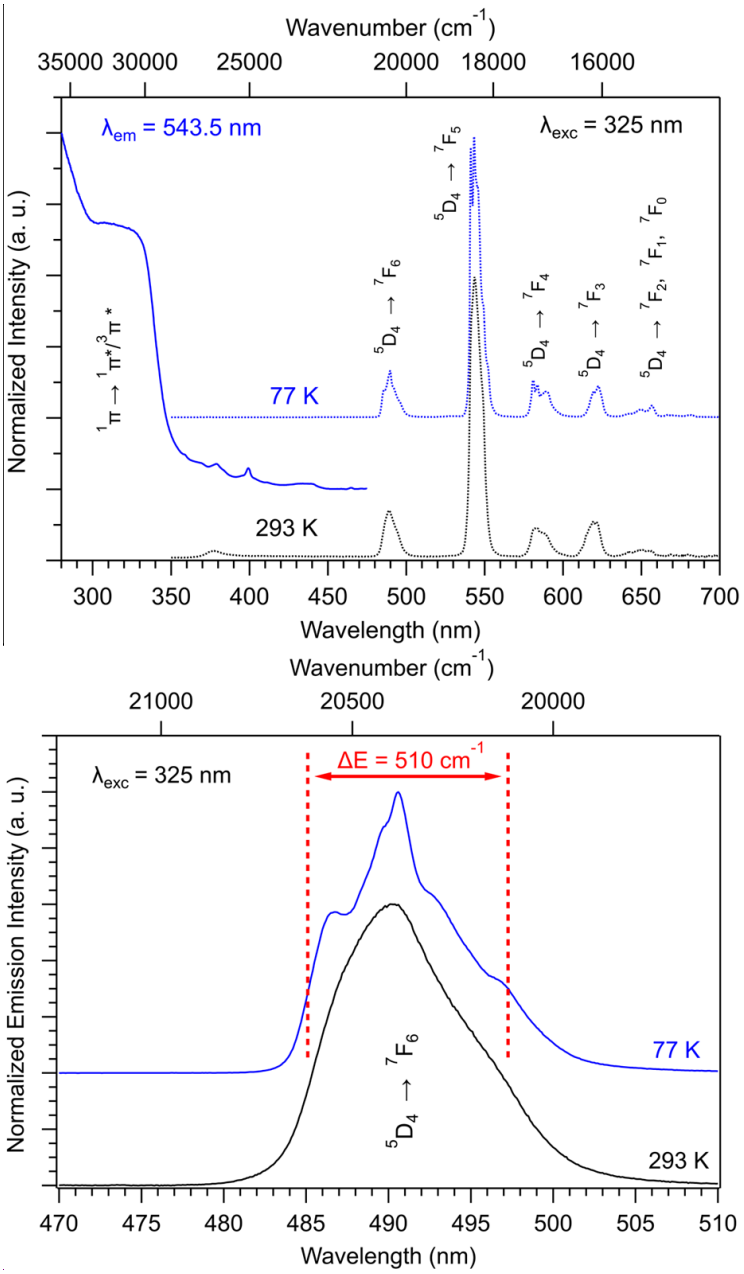

Figure 7. (top) Solid state emission (dotted) and excitation (full line) measured at 77 K (blue curves) and 293 K (black curve) on a single-crystal of **Tb-TEMPO-CN** reported with the associated transitions. (Bottom) Highlight of the $^5D_4 \rightarrow {}^7F_6$ transition for various temperatures and estimation of $^7F_6$ splitting upon photo-excitation at 325 nm.

Dynamic magnetic properties

Dynamic magnetic measurements have been performed on **Dy-TEMPO-CN** and **Tb-TEMPO-CN**.

On the Dy derivative no zero-field χ_M" signal has been observed. An optimum dc field of H_{dc} = 2400 Oe was necessary to remove fast relaxing processes in the sample (Figure S8). Two sets of peaks can be observed, in line with the presence of two different Dy ions in the crystal structure (Figure 8 and S9). The extraction of the relaxation times (τ) in an Arrhenius plot ($\ln\tau$ vs T^{-1}) affords two linear regimes that can be fitted tentatively considering an Orbach relaxation process ($\tau = \tau_0 \exp(U_{eff}/k_BT)$, with τ_0 the characteristic relaxation time and U_{eff} the effective energy barrier for spin reversal). Given the crossover between the two regimes it has been impossible to consider additional relaxation processes (Raman, …) without reasonable errors. Fitting provides U_{eff} = 11.3 ± 0.7 K with τ_0 = 1.04 x 10^{-5} s for the low temperature regime and U_{eff} = 8.9 ± 0.5 K with τ_0 = 1.10 x 10^{-5} s for the high temperature regime (Figure 9, Table S4). The two relaxation regimes are also clearly evidenced on Cole-Cole plots (Figure 9, Table S5). These plots allow estimating the distribution of the relaxation times in the sample with $0 < \alpha < 1$ for a single ($\alpha = 0$) or an infinite distribution of the relaxation times ($\alpha = 1$). On **Dy-TEMPO-CN**, α values are quite high with $0.48 < \alpha < 0.56$ and $0.27 < \alpha < 0.39$ for the low and high temperature regimes, respectively.

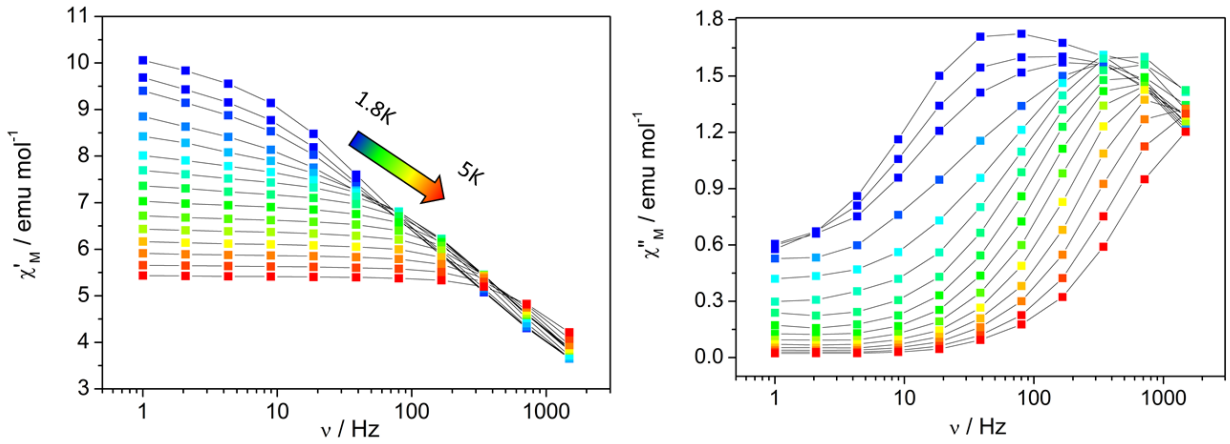

Figure 8. Frequency dependence of the in-phase (left) and out-of-phase (right) magnetic susceptibility of **Dy-TEMPO-CN** (H_{dc} = 2400 Oe). Temperature plots of these data are available in Figure S9. Lines are guides to the eye.

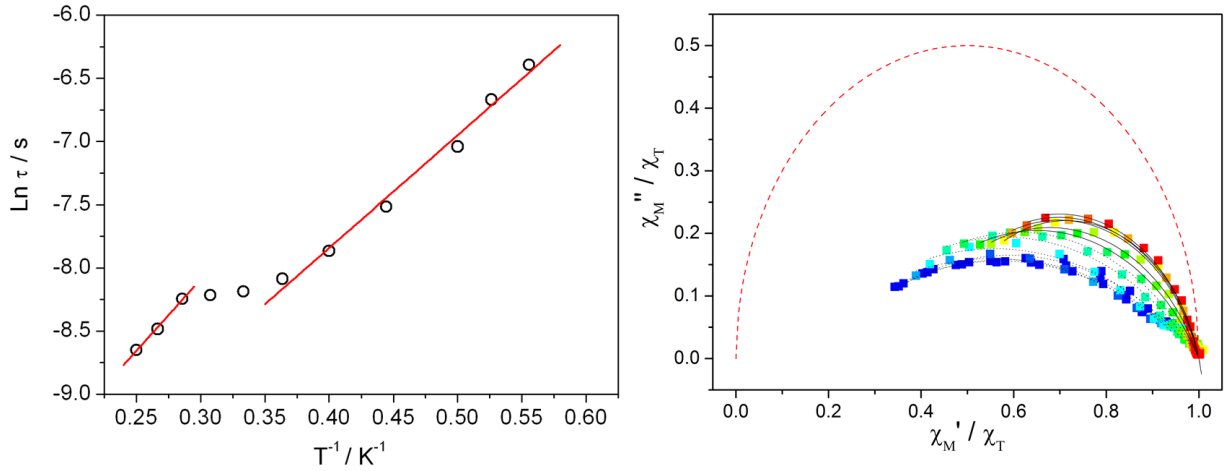

Figure 9. (left) Plot of ln(τ) versus (T^{-1}) for complex **Dy-TEMPO-CN** with fits of Orbach relaxation as red lines. (right) Normalized Cole-Cole plots for **Dy-TEMPO-CN**. Color mapping from 1.8 K (blue) to 4.5 K (red). Black doted lines represent the fits of low temperature process, black full lines stand for the fits of high temperature process. The dashed lines represent the ideal single-relaxation process (α = 0) with 100% relaxing fraction (1-(χ_S/χ_T) = 0).

The Tb derivative (**Tb-TEMPO-CN**) shows significantly better magnetic slow relaxation than **1**. Under an optimum dc fied of 2000 Oe (Figure S10) frequency dependence of ac signals is observed for temperatures as high as 10 K (Figure 10). Extraction of the relaxation times (Table S6) affords an Arrhenius plot whose high temperature regime ($8 < T < 10$ K) can be fitted considering an Orbach relaxation process to afford $U_{eff} = 69.3 \pm 1$ K which is among the highest values for a Tb-nitroxide or Tb-nitronyl-nitroxide compound (see Table 3) associated with $\tau_0 = 1.31 \times 10^{-7}$ s. These findings confirm that strong interaction between Tb^{III} ion and S = 1/2 spin carriers such as radicals or Cu^{II} ions[96] leads to remarkable SMM behavior. At lower temperature ($T < 6$ K) another linear regime is observed ($U_{eff} = 20.1 \pm 0.2$, $\tau_0 = 1.9 \times 10^{-4}$ s). It is worth noticing that any attempts to fit the extracted relaxation times (τ) over the whole investigated temperature range failed even considering combinations of various relaxation processes. The low temperature regime is then related to a magnetic object that is severely affected by interchain interactions. This is in line with static magnetic measurement where a kink at 6 K is observed (Figure 5). This also recalls the observation made on **Gd-TEMPO-CN** where sizeable interchain interaction has been quantified below 6 K (Figure 4). Last, this is in agreement with our recent study that demonstrates that small interchain dipolar couplings at relatively long distances have a significant impact on the magnetic relaxation of lanthanide ions.[97]

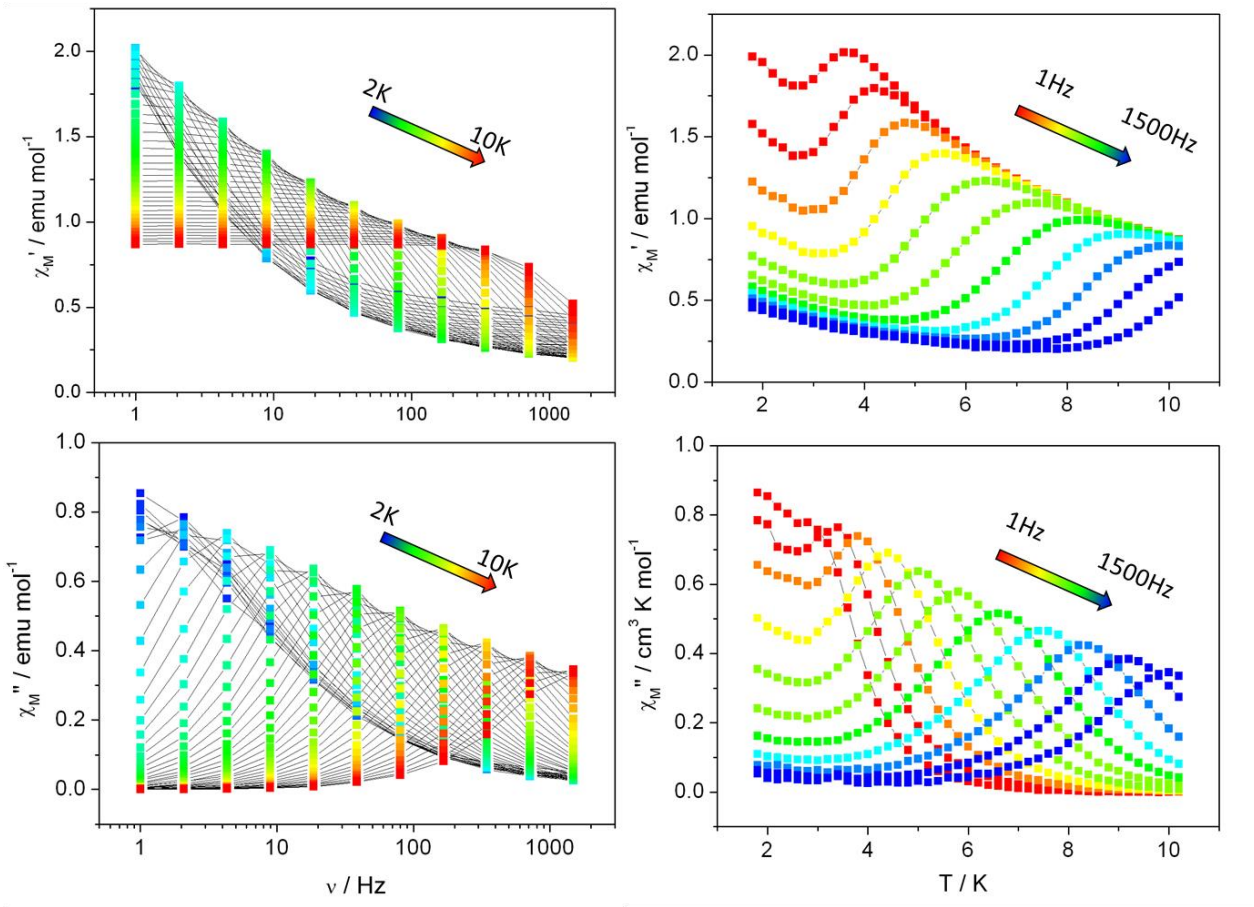

Figure 10. (left) Frequency dependence of the in-phase (top) and out-of-phase (bottom) magnetic susceptibility for **Tb-TEMPO-CN** (H_{dc} = 2000 Oe). (right) Temperature dependence of the in-phase (top) and out-of-phase (bottom) magnetic susceptibility of **Tb-TEMPO-CN** (H_{dc} = 2000 Oe). Lines are guides to the eye.

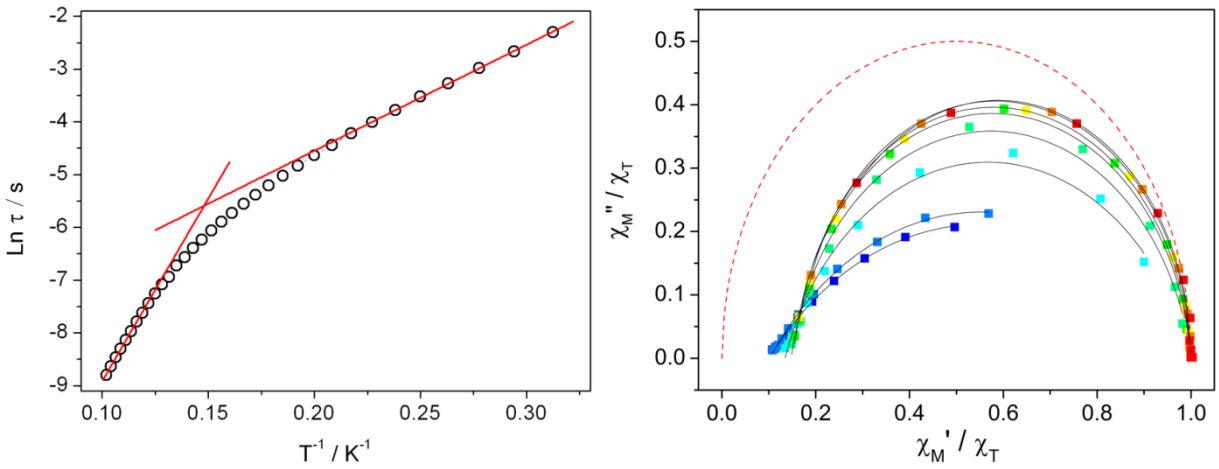

Figure 11. (left) Plot of ln(τ) versus (T^{-1}) for **Tb-TEMPO-CN** with the two linear regimes fitted as red lines. (right) Normalized Cole-Cole plots for **Tb-TEMPO-CN** with color mapping from 2 K (blue) to 10 K (red); the dashed lines represent the ideal single-relaxation process (α = 0) with 100% relaxing fraction (1-(χ_S/χ_T) = 0).

No further flattening of the Arrhenius plot is observed at low temperature suggesting that the combination of the Tb-radical magnetic coupling and the applied dc field efficiently suppresses quantum tunneling in **Tb-TEMPO-CN.** This prompted us to perform low temperature (T = 0.5 K) hysteresis measurement and a very small opening of magnetic hysteresis loop is observed around 2000 Oe (Figure S11).

In order to confirm these findings Cole-Cole plots have been fitted (Figure 11, Table S7) and two regimes can be observed. At high temperature low α values (α_{9K} = 0.005) associated with a relaxing fraction of (1-(χ_S/χ_T)) = 82% (with χ_S the adiabatic, χ_T the isotherm susceptibility and (1-(χ_S/χ_T)) represents the amount of sample that undergoes magnetic slow relaxation) are observed. In the low temperature regime (T < 6 K) a better relaxing fraction is observed (ca

90%) but with higher α, (α_{2K} = 0.44). This is in line with the presences of several interchain interactions below 6 K that broadens the relaxation times distribution.

Table 3. Spin relaxation barrier (U_{eff}) and pre-exponential factors (τ_0) for Tb-radical SMMs (modified and completed from Ref. [9]).

Compound	Structure	H_{dc} (kOe)	U_{eff} (K)	τ_0 (s)	Ref
Phthalocyanines					
Tb(Pc)(Pc(O(C_6H_4)-*p*-*t*Bu)$_8$)	Mononuclear	0	652	1.1 x 10^{-11}	98
Tb(Pc)(Pc(*t*Bu)$_4$)	Mononuclear	0	642	2.2 x 10^{-11}	98
Tb[Pc(O(C_6H_4)-*p*-*t*Bu)$_8$]$_2$	Mononuclear	0	504	2.2 x 10^{-11}	98
[Tb(Pc(S-DOP)$_8$)$_2$]$_{cr}$	Mononuclear	0	480	6.9 x 10^{-12}	99
[Tb(Pc(S-DOP)$_8$)$_2$]$_{dis}$	Mononuclear	0	422	1.7 x 10^{-10}	99
$TbPc_2$	Mononuclear	0	410	1.5 x 10^{-9}	100
(Pc)Tb[Pc[N-(C_4H_9)$_2$]$_8$]	Mononuclear	0	657	8.9 x 10^{-13}	101
((15-C-5)$_4$Pc)Tb	Dinuclear	0	350	1.93 x 10^{-9}	102
[(((15-C-5)$_4$Pc)Tb)$_2$$K_4$]$^{4+}$	Dinuclear	0	360	4.42 x 10^{-9}	102
2,3,5,6-tetra(2-pyridyl)-pyrazine (tppz)					
[(Cp*$_2$Tb)$_2$(μ-tppz$^{\bullet}$)]$^+$	Dinuclear	0	5.1	6 x 10^{-6}	103
Bipyrimidyls					
[(Cp*$_2$Tb)$_2$(μ-bpym$^{\bullet}$)]$^+$	Dinuclear	0	44	4 x 10^{-8}	104
N_2^{3-}					
[K(18-C-6)][((Me$_3$Si)$_2$N)$_2$(THF)Tb]$_2$($N_2^{\bullet}$)	Dinuclear	0	227	8.2 x 10^{-9}	105
[K][((Me$_3$Si)$_2$N)$_2$(THF)Tb]$_2$($N_2^{\bullet}$)	Dinuclear	0	41	3.9 x 10^{-6}	76
[(Cp^{Me4H}$_2$Tb(THF))$_2$(μ−$N_2^{\bullet}$)]$^-$	Dinuclear	0	242	1.4 x 10^{-9}	14
[(Cp^{Me4H}$_2$Tb)$_2$(μ−$N_2^{\bullet}$)]$^-$	Dinuclear	0	276	1.3 x 10^{-9}	14
Nitronyl-Nitroxides					

$Tb(hfac)_3(NITPhOEt)_2$	Mononuclear	0	20	3×10^{-8}	[106]
$[Tb(hfac)_3(NIT\text{-}5\text{-}Py\text{-}3Br)]_2$	Dinuclear	0	20	5.9×10^{-9}	[107]
$Tb(acac)_3NIT2Py \bullet 0.5H_2O$	Mononuclear	1, 3.5	15, 18	1×10^{-7}, 3×10^{-8}	[108]
$[Tb(Phtfac)_3(NIT4Py)]_2$	Dinuclear	0	18	4.1×10^{-8}	[109]
$[Tb(hfac)_3(NITPhPO(OEt)_2)]_2$	Dinuclear	2	17, 15	$3.4 \times 10^{-9}/1.8 \times 10^{-9}$	[110]
$Tb(NITpic)_3$	Mononuclear	0	16	5.5×10^{-9}	[111]
$[Tb(hfac)_3(NIT3Py)]_2$	Dinuclear	3	13	8.8×10^{-8}	[112]
$[Tb(hfac)_3(NIT2Py)] \cdot 0.5C_7H_{16}$	Mononuclear	0	12	9.6×10^{-7}	[113]
$[Tb(hfac)_3(5\text{-}IndazoleNIT)]_2$	Dinuclear	0	2.5	1.8×10^{-7}	[114]
$Tb(tfa)_3NITBzImH$	Mononuclear	0	10	4.6×10^{-7}	[115]
$[Tb(hfac)_3NITPhOPh]_n$	Chain	0	31.2 *	9.6×10^{-9}	[58]
$[Tb(hfac)_3NIT\text{-}2thien]_n$	Chain	0	54	1.9×10^{-9}	[116]
$[Tb(hfac)_3NIT\text{-}3Brthien]_n$	Chain	0	40	1.1×10^{-8}	[117]
$[Tb(hfac)_3NIT\text{-}I]_n$	Chain	0	49	7.1×10^{-10}	[118]
$[Tb(hfac)_3NIT_3BrPhOMe]_n$	Chain	0	41	2.3×10^{-7}	[79]
$[Tb(hfac)_3(NITPh\text{-}2OEt)]_n$	Chain	0	39	9.7×10^{-10}	[119]
$[Tb(hfac)_3(NIT\text{-}C_3H_5)]n$	Chain	1	7	9×10^{-6}	[120]
$[Tb(hfac)_3(NIT\text{-}CH_3)]n$	Chain	1	5	8×10^{-7}	[120]
$Tb(tfa)_3(NITPhImbis)] \cdot CH_2Cl_2$	Chain	0	9	7.8×10^{-7}	[121]
$[Tb(hfac)_3(NITPhCOOMe)]_n$	Chain	1	25	9.2×10^{-7}	[122]
Nitroxides					
$Tb(hfac)_3(2PyNO)$	Mononuclear	0	25/27	$4.1 \times 10^{-7}/4.2 \times 10^{-8}$	[40]
$Tb(hfac)_3(PhNO)(H_2O)$	Mononuclear	2	21/46	$1.3 \times 10^{-8}/1.9 \times 10^{-9}$	[37]
$Tb(hfac)_3(6bpyNO)]$	Mononuclear	2	14.7	1.7×10^{-9}	[38]
Tb-TEMPO-CN	Chain	2	69.3/20.1	$1.93 \times 10^{-7}/1.9 \times 10^{-4}$	This work

*Single-Chain Magnet

Abbreviations: Pc = phthalocyaninate, tBu = *tert*-butyl, S-DOP = S-dodexyloxypropane, hfac = (1,1,1,5,5,5)-hexafluoroacetylacetonate, acac = acetylacetonate, tfa = trifluoroacetylacetonate, NITPhOEt = 4'-ethoxy-phenyl-4,4,5,5-tetramethylimidazoline-1-oxyl-3-oxide, NIT-5-Py-3Br = 2-(5-bromo-3-pyridine)-4,4,5,5-tetramethyl-4,5-dihydro1-H-imidazolyl-1-oxy-3-oxide, NIT2Py = 2-(2'-pyridyl)-4,4,5,5-tetramethyl-4,5-dihydro1-H-imidazolyl-1-oxy-3-oxide, Phtfac = phenyltrifluoroacetylacetonate, NIT4Py = 2-(4'-pyridyl)-4,4,5,5-tetramethyl-4,5-dihydro1-H-imidazolyl-1-oxy-3-oxide, NITPhPO(OEt)2 = (diethoxylphosphine oxide)-4′-phenyl-4,4,5,5-tetramethylimidazoline-1-oxyl-3-oxide, NIT3Py = 2-(3'-pyridyl)-4,4,5,5-tetramethyl-4,5-dihydro1-H-imidazolyl-1-oxy-3-oxide, NITpic = picolinate-4,4,5,5-tetramethyl-4,5-dihydro1-H-imidazolyl-1-oxy-3-oxide, NITBzImH = 2-(2-benz-imidazolyl)-4,4,5,5-tetramethyl-4,5-dihydro-1H-imidazolyl-3-oxide-1-oxide, NITPhOPh = 2,4'-benzoxo-4,4,5,5-tetramethylimidazoline-1-oxyl-3-oxide, NIT-2thien = 2-(2'-thienyl)-4,4,5,5-tetramethyl-imidazoline-1-oxyl-3-oxide, NIT-3Brthien = 2-(3'-bromo-20-thienyl)-4,4,5,5-tetramethyl-imidazoline-1-oxyl-3-oxide), NIT-Ph-2OEt = 2-(2′-ethoxyphenyl)-4,4,5,5-tetramethylimidazoline-1-oxyl-3-oxide), NIT5-Indazole = 5-(1′-oxyl-3′-oxido-4′,4′,5′,5′-tetramethyl- 4,5-hydro-1H-imidazol-2-yl)-1H-indazole), NIT-3Brthien = 2-(3'-bromo-20-thienyl)-4,4,5,5-tetramethyl-imidazoline-1-oxyl-3-oxide), NIT-I = 2-iodo-4,4,5,5-tetramethylimidazoline-1-oxyl-3-oxide, 2PyNO = *tert*-butyl 2-pyridyl nitroxide, NITPhImbis = 1-imidazole-3,5-bis(1'-oxyl-30-oxido-4',4',5',5'-tetramethyl-4,5-hydro-1H-imidazol-2-yl)benzene, NITPhCOOMe = 2-(4-(methoxycarbonyl)phenyl)-4,4,5,5-tetramethylimidazolin-1-oxyl-3-oxide), 6bpyNO = 2,2'-bipyridin-6-yl-*tert*-butyl nitroxide), phNO = *tert*-butyl phenyl nitroxide, TEMPO = 2,2,6,6-tetramethylpiperidine 1-Oxyl.

CONCLUSION

In this study Ln^{III} ions have been associated with TEMPO-CN radical with the aim of building molecular magnetic chains. Indeed the CN group of the radical ligand is able to bind Gd^{III} and Tb^{III} ions to form 1D molecular edifice in which strong Ln-radical AF interaction is observed. For **Gd-TEMPO-CN** the coupling is $J_{Gd\text{-}rad} = -21.18$ K (zJ' = -0.029 K) the highest Gd-radical coupling ever reported with nitroxide-based radicals. **Tb-TEMPO-CN** shows a similar behavior with $J_{Tb\text{-}rad} = -23.02$ K estimated from ab-initio calculations. Magneto-luminescent correlations have been undertaken and single-crystal luminescence measurements of the overall splitting of the $^7F_6$ ground state well match with the one found via ab-initio calculations. Additionally **Tb-TEMPO-CN** shows significant SMM behavior for Ln-radical-based compound with $U_{eff} = 69.3 \pm 1$ K and $\tau_0 = 1.31 \times 10^{-7}$ s. These findings are extremely promising for the design of new air and moisture stable magnetic materials and propose TEMPO radicals as an efficient alternative to the widely used nitronyl-nitroxide radicals.

ASSOCIATED CONTENT

Supporting Information.

Selected bonds and angles, CSM factor data, crystal packing views, additional magnetic data, additional luminescent measurements, crystallographic data files. The Supporting Information is available free of charge on the ACS Publications website.

AUTHOR INFORMATION

Corresponding Author

*E-mail: kevin.bernot@insa-rennes.fr

Notes

The authors declare no competing financial interest

ACKNOWLEDGMENT

We acknowledge financial support from Chinese Scolarship Council (CSC) and Rennes Metropole. K.B. thanks Institut Universitaire de France (IUF). B.L.G. thanks the French GENCI/IDRIS-CINES center for high-performance computing resources.

REFERENCES

(1) Rajeshkumar, T.; Rajaraman, G. Is a radical bridge a route to strong exchange interactions in lanthanide complexes? A computational examination. *Chem. Commun.* **2012**, *48*, 7856-7858.

(2) Kanetomo, T.; Yoshitake, T.; Ishida, T. Strongest Ferromagnetic Coupling in Designed Gadolinium(III)–Nitroxide Coordination Compounds. *Inorg. Chem.* **2016**, *55*, 8140-8146.

(3) Nakamura, T.; Ishida, T. Strong exchange couplings in lanthanide complexes with an aliphatic nitroxide radical 1,1,3,3-tetramethylisoindolin-2-oxyl. *Polyhedron* **2015**, *87*, 302-306.

(4) Harriman, K. L. M.; Brosmer, J. L.; Ungur, L.; Diaconescu, P. L.; Murugesu, M. In the Pursuit of Record Breaking Energy Barriers: A Study of Magnetic Axiality in Diamide Ligated DyIII Single-Molecule Magnets. *J. Am. Chem. Soc.* **2017**, *139*, 1420-1423.

(5) Goodwin, C. A. P.; Ortu, F.; Reta, D.; Chilton, N. F.; Mills, D. P. Molecular magnetic hysteresis at 60 kelvin in dysprosocenium. *Nature* **2017**, *548*, 439-442.

(6) Chen, Y.-C.; Liu, J.-L.; Lan, Y.; Zhong, Z.-Q.; Mansikkamäki, A.; Ungur, L.; Li, Q.-W.; Jia, J.-H.; Chibotaru, L. F.; Han, J.-B.; Wernsdorfer, W.; Chen, X.-M.; Tong, M.-L. Dynamic Magnetic and Optical Insight into a High Performance Pentagonal Bipyramidal Dy(III) Single-Ion Magnet. *Chem. Eur. J.* **2017**, *23*, 5708-5715.

(7) Pugh, T.; Chilton, N. F.; Layfield, R. A. A Low-Symmetry Dysprosium Metallocene Single-Molecule Magnet with a High Anisotropy Barrier. *Angew. Chem.-Int. Ed.* **2016**, *55*, 11082-11085.

(8) Liu, J.; Chen, Y.-C.; Liu, J.-L.; Vieru, V.; Ungur, L.; Jia, J.-H.; Chibotaru, L. F.; Lan, Y.; Wernsdorfer, W.; Gao, S.; Chen, X.-M.; Tong, M.-L. A Stable Pentagonal Bipyramidal Dy(III) Single-Ion Magnet with a Record Magnetization Reversal Barrier over 1000 K. *J. Am. Chem. Soc.* **2016**, *138*, 5441-5450.

(9) Demir, S.; Jeon, I.-R.; Long, J. R.; Harris, T. D. Radical ligand-containing single-molecule magnets. *Coord. Chem. Rev.* **2015**, *289–290*, 149-176.

(10) Preuss, K. E. Metal-radical coordination complexes of thiazyl and selenazyl ligands. *Coord. Chem. Rev.* **2015**, *289–290*, 49-61.

(11) Benelli, C.; Caneschi, A.; Gatteschi, D.; Pardi, L. One-dimensional magnetic materials with dominant next-nearest-neighbor interactions. *J. Appl. Phys.* **1990**, *67*, 5613-5615.

(12) Caneschi, A.; Gatteschi, D.; Lalioti, N.; Sangregorio, C.; Sessoli, R.; Venturi, G.; Vindigni, A.; Rettori, A.; Pini, M. G.; Novak, M. A. Glauber slow dynamics of the magnetization in a molecular Ising chain. *Europhys. Lett.* **2002**, *58*, 771-777.

(13) Guo, F.-S.; Layfield, R. A. Strong direct exchange coupling and single-molecule magnetism in indigo-bridged lanthanide dimers. *Chem. Commun.* **2017**, *53*, 3130-3133.

(14) Demir, S.; Gonzalez, M. I.; Darago, L. E.; Evans, W. J.; Long, J. R. Giant coercivity and high magnetic blocking temperatures for N_2^{3-} radical-bridged dilanthanide complexes upon ligand dissociation. *Nat. Commun.* **2017**, *8*, 2144.

(15) Rinehart, J. D.; Fang, M.; Evans, W. J.; Long, J. R. Strong exchange and magnetic blocking in N(2)(3-)-radical-bridged lanthanide complexes. *Nat. Chem.* **2011**, *3*, 538-542.

(16) Ohira, S.; Nakayama, K.; Ise, T.; Ishida, T.; Nogami, T.; Watanabe, I.; Nagamine, K. Anomalous magnetism in organic radical ferromagnets 4-arylmethyleneamino-2,2,6,6-tetramethylpiperidin-1-yloxyl just above TC studied by the μSR method. *Polyhedron* **2001**, *20*, 1223-1227.

(17) Ishida, T.; Ohira, S.; Watanabe, I.; Nogami, T.; Nagamine, K. Zero-field muon spin rotation study on TEMPO-based magnets, Ar-CH□N-TEMPO. *Polyhedron* **2001**, *20*, 1545-1549.

(18) Takahashi, M.; Turek, P.; Nakazawa, Y.; Tamura, M.; Nozawa, K.; Shiomi, D.; Ishikawa, M.; Kinoshita, M. Discovery of a quasi-1D organic ferromagnet, p-NPNN. *Phys. Rev. Lett.* **1991**, *67*, 746-748.

(19) Benelli, C.; Gatteschi, D. Magnetism of Lanthanides in Molecular Materials with Transition-Metal Ions and Organic Radicals. *Chem. Rev.* **2002**, *102*, 2369-2388.

(20) Lescop, C.; Bussiere, G.; Beaulac, R.; Belisle, H.; Belorizky, E.; Rey, P.; Reber, C.; Luneau, D. Magnetic and optical properties of nitroxide radicals and their lanthanide complexes. *J. Phys. Chem. Solids* **2004**, *65*, 773-779.

(21) Luneau, D.; Rey, P. Magnetism of metal-nitroxide compounds involving bis-chelating imidazole and benzimidazole substituted nitronyl nitroxide free radicals. *Coord. Chem. Rev.* **2005**, *249*, 2591-2611.

(22) Xu, J.-X.; Ma, Y.; Xu, G.-F.; Wang, C.; Liao, D.-Z.; Jiang, Z.-H.; Yan, S.-P.; Li, L.-C. A four-spin ring with alternating magnetic interactions formed by pyridine-substituted nitronyl nitroxide radicals and Gd(III) ions: Crystal structure and magnetic properties. *Inorg. Chem. Commun.* **2008**, *11*, 1356-1358.

(23) Benelli, C.; Caneschi, A.; Gatteschi, D.; Laugier, J.; Rey, P. Structure and magnetic-properties of a gadolinium hexafluoroacetylacetonate adduct with the radical 4,4,5,5-tetramethyl-2-phenyl-4,5-dihydro-1H-imidazole-3-oxide-1-oxyl. *Angew. Chem.-Int. Edit. Engl.* **1987**, *26*, 913-915.

(24) Zhou, N.; Ma, Y.; Wang, C.; Xu, G.-F.; Tang, J.; Yan, S.-P.; Liao, D.-Z. Two tri-spin complexes based on gadolinium and nitronyl nitroxide radicals: Structure and ferromagnetic interactions. *J. Solid State Chem.* **2010**, *183*, 927-932.

(25) Lescop, C.; Luneau, D.; Belorizky, E.; Fries, P.; Guillot, M.; Rey, P. Unprecedented Antiferromagnetic Metal−Ligand Interactions in Gadolinium−Nitroxide Derivatives. *Inorg. Chem.* **1999**, *38*, 5472-5473.

(26) Lescop, C.; Belorizky, E.; Luneau, D.; Rey, P. Synthesis, Structures, and Magnetic Properties of a Series of Lanthanum(III) and Gadolinium(III) Complexes with Chelating Benzimidazole-Substituted Nitronyl Nitroxide Free Radicals. Evidence for Antiferromagnetic GdIII−Radical Interactions. *Inorg. Chem.* **2002**, *41*, 3375-3384.

(27) Benelli, C.; Caneschi, A.; Gatteschi, D.; Pardi, L.; Rey, P.; Shum, D. P.; Carlin, R. L. Magnetic properties of lanthanide complexes with nitronyl nitroxides. *Inorg. Chem.* **1989**, *28*, 272-275.

(28) Benelli, C.; Caneschi, A.; Gatteschi, D.; Pardi, L.; Rey, P. Structure and Magnetic Properties of Linear Chain Complexes of Rare Earth Ions (Gadolinium, Europium) with Nitronyl Nitroxides. *Inorg. Chem.* **1989**, *28*, 275.

(29) Benelli, C.; Caneschi, A.; Gatteschi, D.; Pardi, L.; Rey, P. Linear-chain gadolinium(III) nitronyl nitroxide complexes with dominant next-nearest-neighbor magnetic interactions. *Inorg. Chem.* **1990**, *29*, 4223-4228.

(30) Benelli, C.; Caneschi, A.; Gatteschi, D.; Pardi, L. Gadolinium(III) complexes with pyridine-substituted nitronyl nitroxide radicals. *Inorg. Chem.* **1992**, *31*, 741-746.

(31) Ishida, T.; Murakami, R.; Kanetomo, T.; Nojiri, H. Magnetic study on radical-gadolinium(III) complexes. Relationship between the exchange coupling and coordination structure. *Polyhedron* **2013**, *66*, 183-187.

(32) Tsukuda, T.; Suzuki, T.; Kaizaki, S. Synthesis, spectroscopic and magnetic properties of lanthanide(III) complexes with a chelated imino nitroxide radical. *Journal of the Chemical Society, Dalton Transactions* **2002**, 1721-1726.

(33) Lescop, C.; Luneau, D.; Rey, P.; Bussière, G.; Reber, C. Synthesis, Structures, and Magnetic and Optical Properties of a Series of Europium(III) and Gadolinium(III) Complexes with Chelating Nitronyl and Imino Nitroxide Free Radicals. *Inorg. Chem.* **2002**, *41*, 5566-5574.

(34) Kahn, M. L.; Sutter, J.-P.; Golhen, S.; Guionneau, P.; Ouahab, L.; Kahn, O.; Chasseau, D. Systematic Investigation of the Nature of The Coupling between a Ln(III) Ion (Ln = Ce(III) to Dy(III)) and Its Aminoxyl Radical Ligands. Structural and Magnetic Characteristics of a Series of {Ln(organic radical)2} Compounds and the Related {Ln(Nitrone)2} Derivatives. *J. Am. Chem. Soc.* **2000**, *122*, 3413-3421.

(35) Sutter, J.-P.; Kahn, M. L.; Golhen, S.; Ouahab, L.; Kahn, O. Synthesis and Magnetic Behavior of Rare-Earth Complexes with N,O-Chelating Nitronyl Nitroxide Triazole Ligands: Example of a [GdIII{Organic Radical}2] Compound with an S=9/2 Ground State. *Chem. Eur. J.* **1998**, *4*, 571-576.

(36) Kanetomo, T.; Kihara, T.; Miyake, A.; Matsuo, A.; Tokunaga, M.; Kindo, K.; Nojiri, H.; Ishida, T. Giant Exchange Coupling Evidenced with a Magnetization Jump at 52 T for a Gadolinium-Nitroxide Chelate. *Inorg. Chem.* **2017**, *56*, 3310-3314.

(37) Kanetomo, T.; Yasui, M.; Ishida, T. Exchange-coupled terbium-radical complex Tb-phNO showing slow reversal of magnetization. *Polyhedron* **2017**, *136*, 30-34.

(38) Kanetomo, T.; Yoshii, S.; Nojiri, H.; Ishida, T. Single-molecule magnet involving strong exchange coupling in terbium(III) complex with 2,2'-bipyridin-6-yl tert-butyl nitroxide. *Inorg. Chem. Front.* **2015**, *2*, 860-866.

(39) Baker, M. L.; Tanaka, T.; Murakami, R.; Ohira-Kawamura, S.; Nakajima, K.; Ishida, T.; Nojiri, H. Relationship between Torsion and Anisotropic Exchange Coupling in a TbIII-Radical-Based Single-Molecule Magnet. *Inorg. Chem.* **2015**, *54*, 5732-5738.

(40) Ishida, T. Spin-Parity Behavior in the Exchange-Coupled Lanthanoid-Nitroxide Molecular Magnets. *IOP Conference Series: Materials Science and Engineering* **2017**, *202*, 012001.

(41) Ishida, T.; Nakamura, T.; Kihara, T.; Nojiri, H. Chemical trend on the lanthanide-radical exchange coupling. *Polyhedron* **2017**, *136*, 149-154.

(42) Rinehart, J. D.; Long, J. R. Exploiting single-ion anisotropy in the design of f-element single-molecule magnets. *Chem. Sci.* **2011**, *2*, 2078-2085.

(43) Faber, R. J.; Markley, F. W.; Weil, J. A. Hyperfine Structure in the Solution ESR Spectrum of Di-tert-butyl Nitroxide. *J. Chem. Phys.* **1967**, *46*, 1652-1654.

(44) Goldman, J.; Petersen, T. E.; Torssell, K.; Becher, J. 19F and 1H NMR and ESR investigations of aryl-t-butyl nitroxides and nitronylnitroxides. *Tetrahedron* **1973**, *29*, 3833-3843.

(45) Ullman, E. F.; Osiecki, J. H.; Boocock, D. G. B.; Darcy, R. Stable free radicals. X. Nitronyl nitroxide monoradicals and biradicals as possible small molecule spin labels. *J. Am. Chem. Soc.* **1972**, *94*, 7049-7059.

(46) Caneschi, A.; Gatteschi, D.; Sessoli, R.; Rey, P. Toward molecular magnets - the metal-radical approach. *Acc. Chem. Res.* **1989**, *22*, 392-398.

(47) Artem'ev, A. V.; Vysotskaya, O. V.; Oparina, L. A.; Bogomyakov, A. S.; Khutsishvili, S. S.; Sterkhova, I. V.; Ovcharenko, V. I.; Trofimov, B. A. New heterospin chain-polymers based on $Cu(hfac)_2$ complex with TEMPO derivatives bearing β-(oxy)acrylate moiety: Synthesis, structural and magnetic properties. *Polyhedron* **2016**, *119*, 293-299.

(48) Reis, S. G.; del Aguila-Sanchez, M. A.; Guedes, G. P.; Ferreira, G. B.; Novak, M. A.; Speziali, N. L.; Lopez-Ortiz, F.; Vaz, M. G. F. Synthesis, crystal structures and magnetic behaviour of four coordination compounds constructed with a phosphinic amide-TEMPO radical and [M(hfac)2] (M = CuII, CoII and MnII). *Dalton Trans.* **2014**, *43*, 14889-14901.

(49) Escobar, L. B. L.; Guedes, G. P.; Soriano, S.; Speziali, N. L.; Jordão, A. K.; Cunha, A. C.; Ferreira, V. F.; Maxim, C.; Novak, M. A.; Andruh, M.; Vaz, M. G. F. New Families of Hetero-tri-spin 2p−3d−4f Complexes: Synthesis, Crystal Structures, and Magnetic Properties. *Inorg. Chem.* **2014**, *53*, 7508-7517.

(50) Murakami, R.; Nakamura, T.; Ishida, T. Doubly TEMPO-coordinated gadolinium(III), lanthanum(III), and yttrium(III) complexes. Strong superexchange coupling across rare earth ions. *Dalton Trans.* **2014**, *43*, 5893-5898.

(51) Karbowiak, M.; Rudowicz, C.; Nakamura, T.; Murakami, R.; Ishida, T. Spectroscopic and magnetic studies of erbium(III)-TEMPO complex as a potential single-molecule magnet: Interplay of the crystal-field and exchange coupling effects. *Chem. Phys. Lett* **2016**, *662*, 163-168.

(52) Woodruff, D. N.; Winpenny, R. E. P.; Layfield, R. A. Lanthanide Single-Molecule Magnets. *Chem. Rev.* **2013**, *113*, 5110-5148.

(53) Pointillart, F.; Cador, O.; Le Guennic, B.; Ouahab, L. Uncommon lanthanide ions in purely 4f Single Molecule Magnets. *Coord. Chem. Rev.* **2017**, *346*, 150-175.

(54) Cucinotta, G.; Perfetti, M.; Luzon, J.; Etienne, M.; Car, P.-E.; Caneschi, A.; Calvez, G.; Bernot, K.; Sessoli, R. Magnetic Anisotropy in a Dysprosium/DOTA Single-Molecule Magnet: Beyond Simple Magneto-Structural Correlations. *Angew. Chem.-Int. Edit.* **2012**, *51*, 1606-1610.

(55) Nakamura, T.; Ishida, T. Magnetic exchange interaction in gadolinium(III) complex having aliphatic nitroxide radical TEMPO. *AIP Conference Proceedings* **2016**, *1709*, 020016.

(56) Reis, S. G.; Briganti, M.; Soriano, S.; Guedes, G. P.; Calancea, S.; Tiseanu, C.; Novak, M. A.; del Águila-Sánchez, M. A.; Totti, F.; Lopez-Ortiz, F.; Andruh, M.; Vaz, M. G. F. Binuclear Lanthanide-Radical Complexes Featuring Two Centers with Different Magnetic and Luminescence Properties. *Inorg. Chem.* **2016**, *55*, 11676-11684.

(57) Sessoli, R.; Bernot, K. In *Lanthanides and Actinides in Molecular Magnetism*; Wiley-VCH Verlag GmbH & Co. KGaA: 2015, p 89-124.

(58) Bernot, K.; Bogani, L.; Caneschi, A.; Gatteschi, D.; Sessoli, R. A Family of Rare-Earth-Based Single Chain Magnets:Playing with Anisotropy. *J. Am. Chem. Soc.* **2006**, *128*, 7947-7956.

(59) Sheldrick, G. M. A short history of SHELX. *Acta Crystallogr. Sect. A* **2008**, *64*, 112-122.

(60) Altomare, A.; Burla, M. C.; Camalli, M.; Cascarano, G. L.; Giacovazzo, C.; Guagliardi, A.; Moliterni, A. G. G.; Polidori, G.; Spagna, R. SIR97: a new tool for crystal structure determination and refinement. *J. Appl. Crystallogr.* **1999**, *32*, 115-119.

(61) Sheldrick, G. M.; Schneider, T. R. SHELXL: High-resolution refinement. *Methods Enzymol.* **1997**, *277*, 319-343.

(62) Farrugia, L. J. WinGX and ORTEP for Windows: an update. *J. Appl. Crystallogr.* **2012**, *45*, 849-854.

(63) Roos, B. O.; Lindh, R.; Malmqvist, P.-Å.; Veryazov, V.; Widmark, P.-O. Main Group Atoms and Dimers Studied with a New Relativistic ANO Basis Set. *J. Phys. Chem. A* **2004**, *108*, 2851-2858.

(64) Malmqvist, P.-Å.; Roos, B. O. The CASSCF state interaction method. *Chem. Phys. Lett* **1989**, *155*, 189-194.

(65) Malmqvist, P. Å.; Roos, B. O.; Schimmelpfennig, B. The restricted active space (RAS) state interaction approach with spin-orbit coupling. *Chem. Phys. Lett* **2002**, *357*, 230-240.

(66) Chibotaru, L. F.; Ungur, L. Ab initio calculation of anisotropic magnetic properties of complexes. I. Unique definition of pseudospin Hamiltonians and their derivation. *J. Chem. Phys.* **2012**, *137*, 064112.

(67) Chibotaru, L. F.; Ungur, L.; Soncini, A. The origin of nonmagnetic Kramers doublets in the ground state of dysprosium triangles: Evidence for a toroidal magnetic moment. *Angew. Chem.-Int. Edit.* **2008**, *47*, 4126-4129.

(68) Ungur, L.; Van den Heuvel, W.; Chibotaru, L. F. Ab initio investigation of the non-collinear magnetic structure and the lowest magnetic excitations in dysprosium triangles. *New J. Chem.* **2009**, *33*, 1224-1230.

(69) Chibotaru, L. F.; Ungur, L.; Aronica, C.; Elmoll, H.; Pilet, G.; Luneau, D. Structure, Magnetism, and Theoretical Study of a Mixed-Valence CoII3CoIII4 Heptanuclear Wheel: Lack of SMM Behavior despite Negative Magnetic Anisotropy. *J. Am. Chem. Soc.* **2008**, *130*, 12445-12455.

(70) Aquilante, F.; Malmqvist, P. Å.; Pedersen, T. B.; Ghosh, A.; Roos, B. O. Cholesky decomposition-based multiconfiguration second-order perturbation theory (CD-CASPT2): Application to the spin-state energetics of Co-III(diiminato)(NPh). *Journal of Chemical Theory and Computation* **2008**, *4*, 694-702.

(71) Roos, B. O.; Lindh, R.; Malmqvist, P. Å.; Veryazov, V.; Widmark, P. O. New relativistic ANO basis sets for transition metal atoms. *Journal of Physical Chemistry A* **2005**, *109*, 6575-6579.

(72) Roos, B. O.; Lindh, R.; Malmqvist, P. Å.; Veryazov, V.; Widmark, P. O.; Borin, A. C. New Relativistic Atomic Natural Orbital Basis Sets for Lanthanide Atoms with Applications to the Ce Diatom and LuF3. *Journal of Physical Chemistry A* **2008**, *112*, 11431-11435.

(73) Alvarez, S.; Alemany, P.; Casanova, D.; Cirera, J.; Llunell, M.; Avnir, D. Shape maps and polyhedral interconversion paths in transition metal chemistry. *Coord. Chem. Rev.* **2005**, *249*, 1693-1708.

(74) Alvarez, S. Polyhedra in (inorganic) chemistry. *Dalton Trans.* **2005**, 2209-2233.

(75) Atwood, D. *The Rare Earth Elements: Fundamentals and Applications*; Wiley 2012.

(76) Meihaus, K. R.; Corbey, J. F.; Fang, M.; Ziller, J. W.; Long, J. R.; Evans, W. J. Influence of an Inner-Sphere K+ Ion on the Magnetic Behavior of N23− Radical-Bridged Dilanthanide Complexes Isolated Using an External Magnetic Field. *Inorg. Chem.* **2014**, *53*, 3099-3107.

(77) Hsu, C.-F.; Lin, S.-H.; Wei, H.-H. Ferromagnetic coupling in a novel dicyanamide-bridged dinuclear gadolinium(III) complex [Gd2(dca)4(OH)2 (NITpPy)4] (NITpPy = 4-pyridyl-nitronyl nitroxide radical). *Inorganic Chemistry Communications* **2005**, *8*, 1128-1132.

(78) Bogani, L.; Vindigni, A.; Sessoli, R.; Gatteschi, D. Single chain magnets: where to from here? *Journal of Materials Chemistry* **2008**, *18*, 4750-4758.

(79) Hu, P.; Wang, X.; Ma, Y.; Wang, Q.; Li, L.; Liao, D. A new family of Ln-radical chains (Ln = Nd, Sm, Gd, Tb and Dy): synthesis, structure, and magnetic properties. *Dalton Trans.* **2014**, *43*, 2234-2243.

(80) Liu, R.; Ma, Y.; Yang, P.; Song, X.; Xu, G.; Tang, J.; Li, L.; Liao, D.; Yan, S. Dynamic magnetic behavior and magnetic ordering in one-dimensional Tb-nitronyl nitroxide radical chain. *Dalton Transactions* **2010**, *39*, 3321-3325.

(81) Kahn, O. *Molecular Magnetism*; Wiley-VCH: Weinheim, 1993.

(82) Gupta, T.; Rajeshkumar, T.; Rajaraman, G. Magnetic exchange in {GdIII-radical} complexes: method assessment, mechanism of coupling and magneto-structural correlations. *Phys. Chem. Chem. Phys* **2014**, *16*, 14568-14577.

(83) Kanetomo, T.; Ishida, T. Strongest Exchange Coupling in Gadolinium(III) and Nitroxide Coordination Compounds. *Inorg. Chem.* **2014**, *53*, 10794-10796.

(84) Kanetomo, T.; Ishida, T. Preparation and characterization of [Gd(hfac)3(DTBN)(H2O)] (DTBN = di-t-butyl nitroxide). Ferromagnetic Gd3+-Gd3+ super-superexchange. *Chem. Commun.* **2014**, *50*, 2529-2531.

(85) Reis, S. G.; Briganti, M.; Martins, D. O. T. A.; Akpinar, H.; Calancea, S.; Guedes, G. P.; Soriano, S.; Andruh, M.; Cassaro, R. A. A.; Lahti, P. M.; Totti, F.; Vaz, M. G. F. First coordination compounds based on a bis(imino nitroxide) biradical and 4f metal ions: synthesis, crystal structures and magnetic properties. *Dalton Trans.* **2016**, *45*, 2936-2944.

(86) Benelli, C.; Gatteschi, D. *Introduction to Molecular Magnetism: From Transition Metals to Lanthanides*; Wiley, 2015.

(87) Patrascu, A. A.; Calancea, S.; Briganti, M.; Soriano, S.; Madalan, A. M.; Cassaro, R. A. A.; Caneschi, A.; Totti, F.; Vaz, M. G. F.; Andruh, M. A chimeric design of heterospin 2p-3d, 2p-4f, and 2p-3d-4f complexes using a novel family of paramagnetic dissymmetric compartmental ligands. *Chem. Commun.* **2017**, *53*, 6504-6507.

(88) Bünzli, J.-C. G. On the design of highly luminescent lanthanide complexes. *Coord. Chem. Rev.* **2015**, *293–294*, 19-47.

(89) Boulon, M. E.; Cucinotta, G.; Luzon, J.; Degl'Innocenti, C.; Perfetti, M.; Bernot, K.; Calvez, G.; Caneschi, A.; Sessoli, R. Magnetic Anisotropy and Spin-Parity Effect Along the Series of Lanthanide Complexes with DOTA. *Angew. Chem.-Int. Edit.* **2013**, *52*, 350-354.

(90) Kishi, Y.; Cornet, L.; Pointillart, F.; Riobé, F.; Lefeuvre, B.; Cador, O.; Guennic, B. L.; Maury, O.; Fujiwara, H.; Ouahab, L. Luminescence and Single-Molecule-Magnet Behaviour in Lanthanide Coordination Complexes Involving Benzothiazole-Based Tetrathiafulvalene Ligands. *Eur. J. Inorg. Chem.* **2018**, *2018*, 458-468.

(91) Soussi, K.; Jung, J.; Pointillart, F.; Le Guennic, B.; Lefeuvre, B.; Golhen, S.; Cador, O.; Guyot, Y.; Maury, O.; Ouahab, L. Magnetic and photo-physical investigations into DyIII and YbIII complexes involving tetrathiafulvalene ligand. *Inorg. Chem. Front.* **2015**, *2*, 1105-1117.

(92) D'Aleo, A.; Pointillart, F.; Ouahab, L.; Andraud, C.; Maury, O. Charge transfer excited states sensitization of lanthanide emitting from the visible to the near-infra-red. *Coord. Chem. Rev.* **2012**, *256*, 1604-1620.

(93) Yi, X.; Bernot, K.; Le Corre, V.; Calvez, G.; Pointillart, F.; Cador, O.; Le Guennic, B.; Jung, J.; Maury, O.; Placide, V.; Guyot, Y.; Roisnel, T.; Daiguebonne, C.; Guillou, O. Unraveling the Crystal Structure of Lanthanide–Murexide Complexes: Use of an Ancient Complexometry Indicator as a Near-Infrared-Emitting Single-Ion Magnet. *Chem. Eur. J.* **2014**, *20*, 1569-1576.

(94) Long, J.; Guari, Y.; Ferreira, R. A. S.; Carlos, L. D.; Larionova, J. Recent advances in luminescent lanthanide based Single-Molecule Magnets. *Coord. Chem. Rev.* **2018**, *363*, 57-70.

(95) Yi, X.; Bernot, K.; Pointillart, F.; Poneti, G.; Calvez, G.; Daiguebonne, C.; Guillou, O.; Sessoli, R. A Luminescent and Sublimable Dy-III-Based Single-Molecule Magnet. *Chem.-Eur. J.* **2012**, *18*, 11379-11387.

(96) Osa, S.; Kido, T.; Matsumoto, N.; Re, N.; Pochaba, A.; Mrozinski, J. A tetranuclear 3d-4f single molecule magnet: [(CuLTbIII)-L-II(hfac)(2)](2). *J. Am. Chem. Soc.* **2004**, *126*, 420-421.

(97) Huang, G.; Fernandez-Garcia, G.; Badiane, I.; Camara, M.; Freslon, S.; Guillou, O.; Daiguebonne, C.; Totti, F.; Cador, O.; Guizouarn, T.; Le Guennic, B.; Bernot, K. Magnetic slow relaxation in a Metal Organic Framework made of chains of ferromagnetically coupled Single-Molecule Magnets. *Chem. Eur. J.* **2018**, *24*, 6983-6991.

(98) Ganivet, C. R.; Ballesteros, B.; de la Torre, G.; Clemente-Juan, J. M.; Coronado, E.; Torres, T. Influence of Peripheral Substitution on the Magnetic Behavior of Single-Ion Magnets Based on Homo- and Heteroleptic TbIII Bis(phthalocyaninate). *Chem. Eur. J.* **2013**, *19*, 1457-1465.

(99) Gonidec, M.; Luis, F.; Vílchez, À.; Esquena, J.; Amabilino, D. B.; Veciana, J. A Liquid-Crystalline Single-Molecule Magnet with Variable Magnetic Properties. *Angew. Chem.-Int. Ed.* **2010**, *49*, 1623-1626.

(100) Ishikawa, N.; Sugita, M.; Tanaka, N.; Ishikawa, T.; Koshihara, S.-y.; Kaizu, Y. Upward Temperature Shift of the Intrinsic Phase Lag of the Magnetization of Bis(phthalocyaninato)terbium by Ligand Oxidation Creating an S = 1/2 Spin. *Inorg. Chem.* **2004**, *43*, 5498-5500.

(101) Chen, Y.; Ma, F.; Chen, X.; Dong, B.; Wang, K.; Jiang, S.; Wang, C.; Chen, X.; Qi, D.; Sun, H.; Wang, B.; Gao, S.; Jiang, J. A New Bis(phthalocyaninato) Terbium Single-Ion Magnet with an Overall Excellent Magnetic Performance. *Inorg. Chem.* **2017**, *56*, 13889-13896.

(102) Horii, Y.; Kishiue, S.; Damjanović, M.; Katoh, K.; Breedlove, B. K.; Enders, M.; Yamashita, M. Supramolecular Approach for Enhancing Single-Molecule Magnet Properties of Terbium(III)-Phthalocyaninato Double-Decker Complexes with Crown Moieties. *Chem. Eur. J.* **2018**.

(103) Demir, S.; Nippe, M.; Gonzalez, M. I.; Long, J. R. Exchange coupling and magnetic blocking in dilanthanide complexes bridged by the multi-electron redox-active ligand 2,3,5,6-tetra(2-pyridyl)pyrazine. *Chem. Sci.* **2014**, *5*, 4701-4711.

(104) Demir, S.; Zadrozny, J. M.; Nippe, M.; Long, J. R. Exchange Coupling and Magnetic Blocking in Bipyrimidyl Radical-Bridged Dilanthanide Complexes. *J. Am. Chem. Soc.* **2012**, *134*, 18546-18549.

(105) Rinehart, J. D.; Fang, M.; Evans, W. J.; Long, J. R. A N(2)(3-) Radical-Bridged Terbium Complex Exhibiting Magnetic Hysteresis at 14 K. *J. Am. Chem. Soc.* **2011**, *133*, 14236-14239.

(106) Zhou, N.; Ma, Y.; Wang, C.; Feng Xu, G.; Tang, J.-K.; Xu, J.-X.; Yan, S.-P.; Cheng, P.; Li, L.-C.; Liao, D.-Z. A monometallic tri-spin single-molecule magnet based on rare earth radicals. *Dalton Trans.* **2009**, 8489-8492.

(107) Xu, J.-X.; Ma, Y.; Liao, D.-z.; Xu, G.-F.; Tang, J.; Wang, C.; Zhou, N.; Yan, S.-P.; Cheng, P.; Li, L.-C. Four New Lanthanide−Nitronyl Nitroxide (LnIII = PrIII, SmIII, EuIII, TmIII) Complexes and a TbIII Complex Exhibiting Single-Molecule Magnet Behavior. *Inorg. Chem.* **2009**, *48*, 8890-8896.

(108) Lannes, A.; Intissar, M.; Suffren, Y.; Reber, C.; Luneau, D. Terbium(III) and Yttrium(III) Complexes with Pyridine-Substituted Nitronyl Nitroxide Radical and Different β-

Diketonate Ligands. Crystal Structures and Magnetic and Luminescence Properties. *Inorg. Chem.* **2014**, *53*, 9548-9560.

(109) Mei, X.-L.; Liu, R.-N.; Wang, C.; Yang, P.-P.; Li, L.-C.; Liao, D.-Z. Modulating spin dynamics of cyclic LnIII-radical complexes (LnIII = Tb, Dy) by using phenyltrifluoroacetylacetonate coligand. *Dalton Trans.* **2012**, *41*, 2904-2909.

(110) Pointillart, F.; Bernot, K.; Poneti, G.; Sessoli, R. Crystal Packing Effects on the Magnetic Slow Relaxation of Tb(III)-Nitronyl Nitroxide Radical Cyclic Dinuclear Clusters. *Inorg. Chem.* **2012**, *51*, 12218-12229.

(111) Coronado, E.; Gimenez-Saiz, C.; Recuenco, A.; Tarazon, A.; Romero, F. M.; Camon, A.; Luis, F. Single-Molecule Magnetic Behavior in a Neutral Terbium(III) Complex of a Picolinate-Based Nitronyl Nitroxide Free Radical. *Inorg. Chem.* **2011**, *50*, 7370-7372.

(112) Tian, H. X.; Liu, R. N.; Wang, X. L.; Yang, P. P.; Li, Z. X.; Li, L. C.; Liao, D. Z. Magnetic Slow Relaxation in Cyclic Tb-III-Nitronyl Nitroxide Radical Complexes. *Eur. J. Inorg. Chem.* **2009**, 4498-4502.

(113) Wang, X.-L.; Li, L.-C.; Liao, D.-Z. Slow Magnetic Relaxation in Lanthanide Complexes with Chelating Nitronyl Nitroxide Radical. *Inorg. Chem.* **2010**, *49*, 4735-4737.

(114) Chen, P. Y.; Shi, X. J.; Li, T.; Tian, L. Two structural analogous TbIII-indazole-radical complexes with different dynamic magnetic behaviors. *Inorg. Chem. Commun.* **2017**, *86*, 58-61.

(115) Hu, P.; Zhu, M.; Mei, X.; Tian, H.; Ma, Y.; Li, L.; Liao, D. Single-molecule magnets based on rare earth complexes with chelating benzimidazole-substituted nitronyl nitroxide radicals. *Dalton Trans.* **2012**, *41*, 14651-14656.

(116) Liu, R. N.; Ma, Y.; Yang, P. P.; Song, X. Y.; Xu, G. F.; Tang, J. K.; Li, L. C.; Liao, D. Z.; Yan, S. P. Dynamic magnetic behavior and magnetic ordering in one-dimensional Tb-nitronyl nitroxide radical chain. *Dalton Trans.* **2010**, *39*, 3321-3325.

(117) Liu, R. N.; Zhang, C. M.; Mei, X. L.; Hu, P.; Tian, H. X.; Li, L. C.; Liao, D. Z.; Sutter, J. P. Slow magnetic relaxation and antiferromagnetic ordering in a one dimensional nitronyl nitroxide-Tb(III) chain. *New J. Chem.* **2012**, *36*, 2088-2093.

(118) Tian, H.; Wang, X.; Mei, X.; Liu, R.; Zhu, M.; Zhang, C.; Ma, Y.; Li, L.; Liao, D. Magnetic Relaxation in TbIII Magnetic Chains with Nitronyl Nitroxide Radical Bridges That Undergo 3D Antiferromagnetic Ordering. *Eur. J. Inorg. Chem.* **2013**, *2013*, 1320-1325.

(119) Li, C.; Sun, J.; Yang, M.; Sun, G.; Guo, J.; Ma, Y.; Li, L. From Monomeric Species to One-Dimensional Chain: Enhancing Slow Magnetic Relaxation through Coupling Mononuclear Fragments in Ln-rad System. *Cryst. Growth Des.* **2016**, *16*, 7155-7162.

(120) Xiao, F.-P.; Hu, P.; Hao, X.-Y.; Cao, J.-F.; Zhu, L.-L. Magnetic relaxation in two 1D Tb-nitronyl nitroxide complexes. *Inorg. Chim. Acta* **2018**, *471*, 608-614.

(121) Li, H.; Sun, J.; Yang, M.; Sun, Z.; Xie, J.; Ma, Y.; Li, L. Functionalized nitronyl nitroxide biradical bridged one-dimensional lanthanide chains: slow magnetic relaxation in the Tb and Dy analogues. *New J. Chem.* **2017**, *41*, 10181-10188.

(122) Li, L.; Liu, S.; Li, H.; Shi, W.; Cheng, P. Influence of external magnetic field and magnetic-site dilution on the magnetic dynamics of a one-dimensional Tb(III)-radical complex. *Chem. Commun.* **2015**, *51*, 10933-10936.

Supplementary Information for

Strong Magnetic Coupling and Single-Molecule Magnet Behavior in Lanthanide-TEMPO radical Chains

*Gang Huang, Carole Daiguebonne, Guillaume Calvez, Yan Suffren, Olivier Guillou, Thierry Guizouarn, Boris Le Guennic, Olivier Cador and Kevin Bernot**

kevin.bernot@insa-rennes.fr

Univ Rennes, INSA Rennes, CNRS, ISCR (Institut des Sciences Chimiques de Rennes) – UMR 6226, F-35000 Rennes, France

Table S1. Selected bond distances and angles for **Dy-TEMPO-CN**.

	Bond lengths (Å)		Angles (°)
Dy1-O1	2.345(4)	O3-Dy1-O1	133.79(13)
Dy1-O2	2.336(3)	O1-Dy1-O1	76.0(2)
Dy1-O4	2.339(3)	O4-Dy1-O1	146.17(14)
Dy1-O3	2.344(3)	O2-Dy1-O3	75.52(12)
Dy2-O11	2.302(4)	O4-Dy1-O3	75.83(13)
Dy2-O10	2.414(3)	N1-O4-Dy1	154.9(4)
Dy2-O6	2.339(3)	O7-Dy2-O5	134.42(12)
Dy2-O8	2.341(3)	O6-Dy2-O10	70.23(13)
Dy2-O7	2.364(3)	O8-Dy2-O7	75.01(12)
Dy2-O12	2.378(3)	O11-Dy2-O9	86.24(15)
Dy2-O5	2.392(4)	O9-Dy2-O12	73.32(13)
Dy2-O9	2.305(3)	O5-Dy2-O9	150.27(12)
		O10-Dy2-O7	76.11(12)
		O8-Dy2-O12	75.48(12)

		O11-Dy2-O6	107.77(14)
		O11-Dy2-O10	71.51(13)

Table S2. Summary of CSM factors extracted with SHAPE [1] for compounds **Dy-TEMPO-CN** and **Tb-TEMPO-CN**.

Compound	Polyhedron	
DyTEMPO-CN Dy1	SAP (D_{4d}) 1.176	TDD (D_{2d}) 0.431
DyTEMPO-CN Dy2	SAP (D_{4d}) 0.937	TDD (D_{2d}) 0.911
TbTEMPO-CN	SAP (D_{4d}) 0.927	TDD (D_{2d}) 1.332

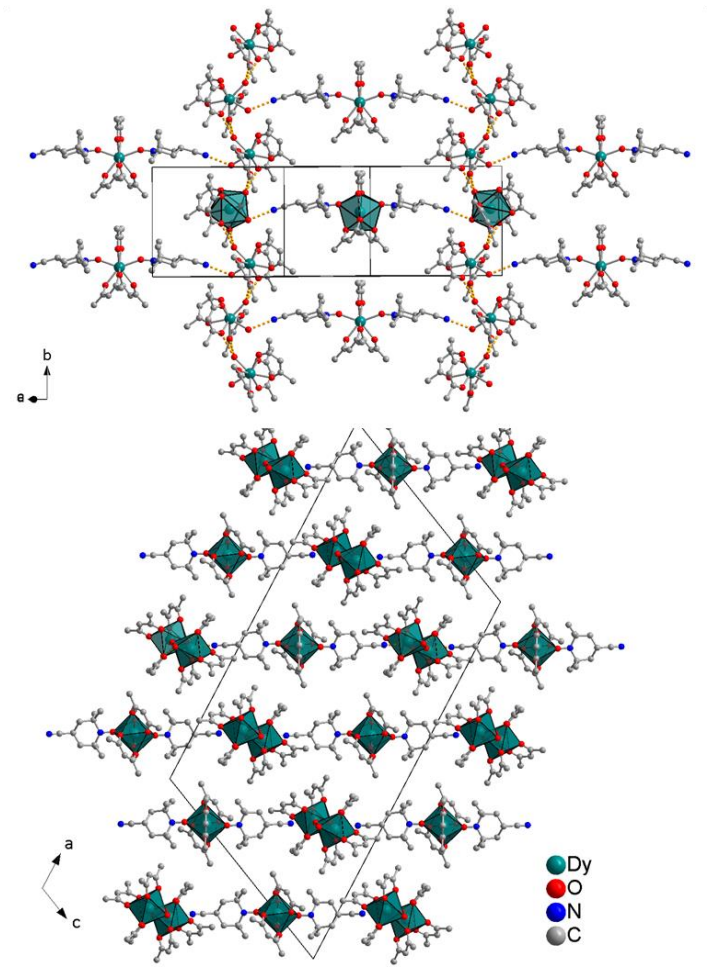

Figure S1. Representation of the crystal packing of **Dy-TEMPO-CN** in the *b*(*a*+*c*) plane (top) and in the *ac* plane (bottom). Hydrogen and fluorine atoms are omitted for clarity.

Table S3. Selected bond distances and angles for **Tb-TEMPO-CN**.

	Bond lengths (Å)		Angles (°)
Tb1-O1	2.345(3)	O1-Tb1-O2	72.64(9)
Tb1-O2	2.346(2)	O6-Tb1-O7	73.35(8)
Tb1-O3	2.330(3)	O4-Tb1-O3	71.9(1)
Tb1-O4	2.387(3)	O3-Tb1-O7	144.85(9)
Tb1-O5	2.289(2)	O1-Tb1-O5	83.93(9)
Tb1-O6	2.376(2)	O5-Tb1-O2	145.05(10)
Tb1-O7	2.337(3)	O2-Tb1-O6	140.03(9)
Tb1-N1	2.541(3)	O7-Tb1-O5	89.81(9)
		O7-Tb1-N1	74.62(10)
		O4-Tb1-O6	128.24(9)
		O3-Tb1-N1	75.45(11)
		O5-Tb1-N1	146.29(10)
		N2-O5-Tb1	176.6(2)

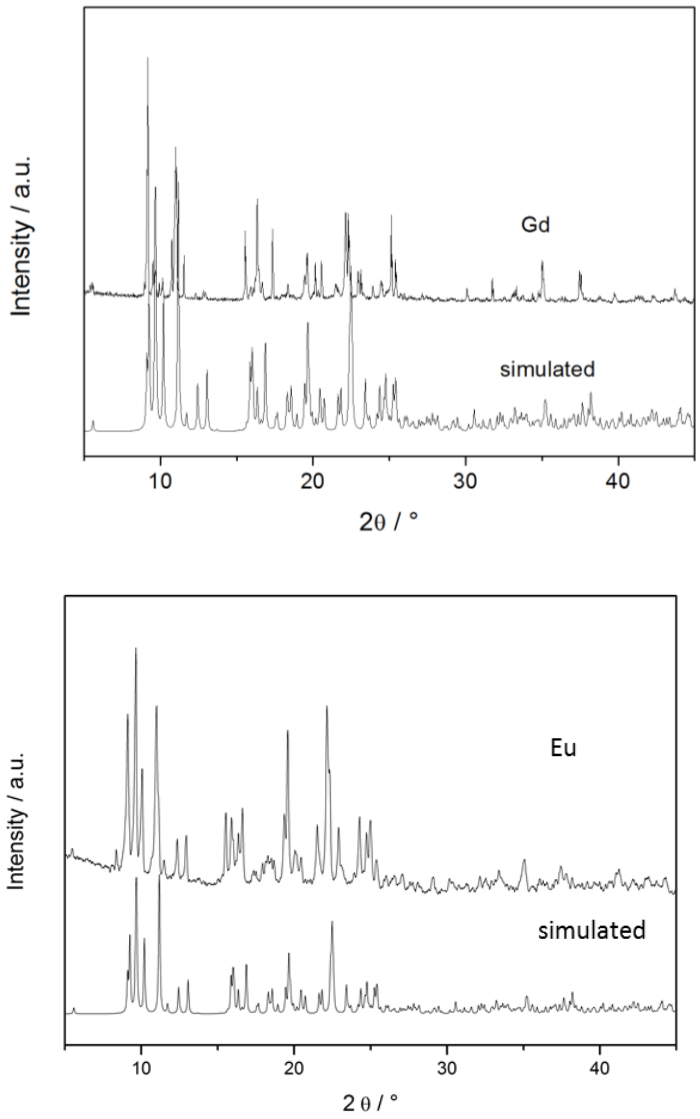

Figure S2. PXRD patterns of the microcrystalline powders of **Gd-TEMPO-CN** (top) and **Eu-TEMPO-CN** (bottom) measured at 300 K and comparison with the simulated pattern from structural data file of **Tb-TEMPO-CN** measured at 150 K.

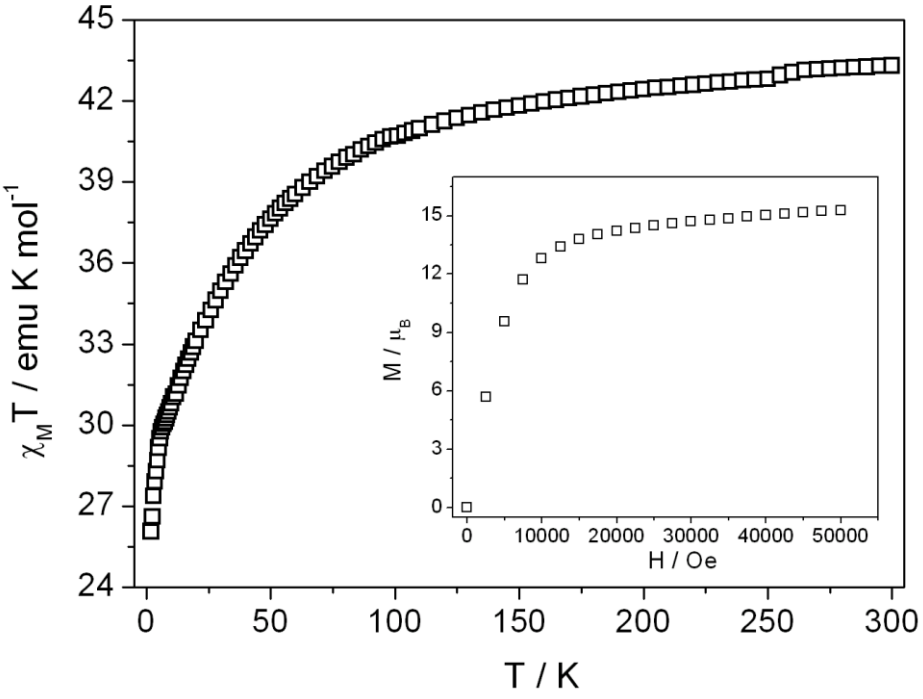

Figure S3. Temperature dependence of the $\chi_M T$ product for **Dy-TEMPO-CN** with magnetization curve at 2 K in inset.

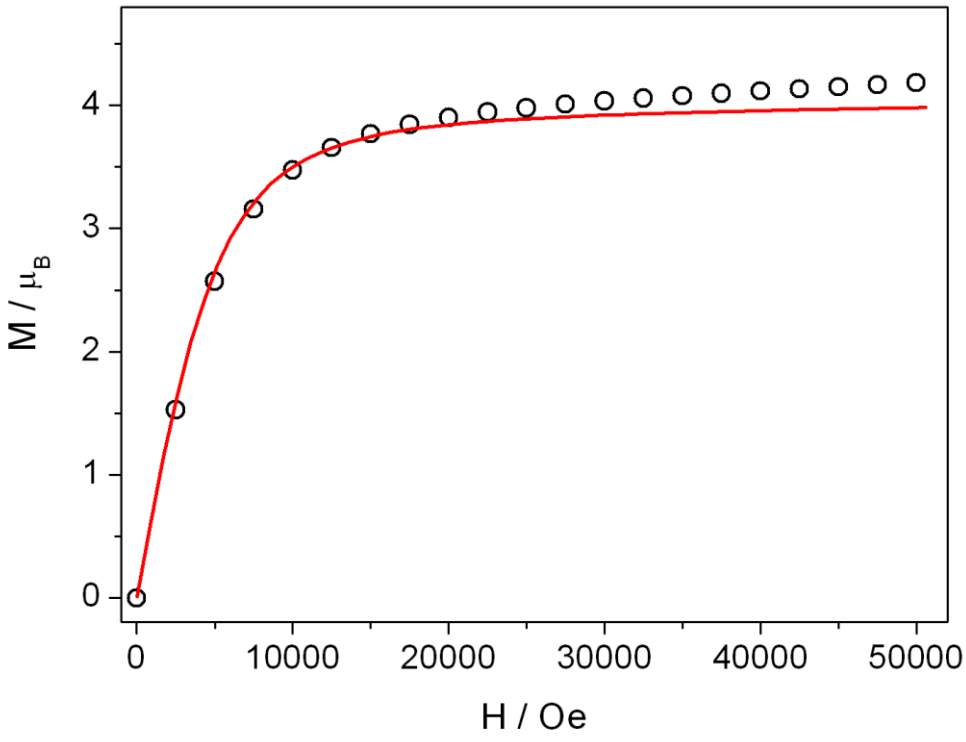

Figure S4. Field variation of the magnetization at 2 K for **Tb-TEMPO-CN** with ab-initio simulation as red curve.

Luminescence measurements

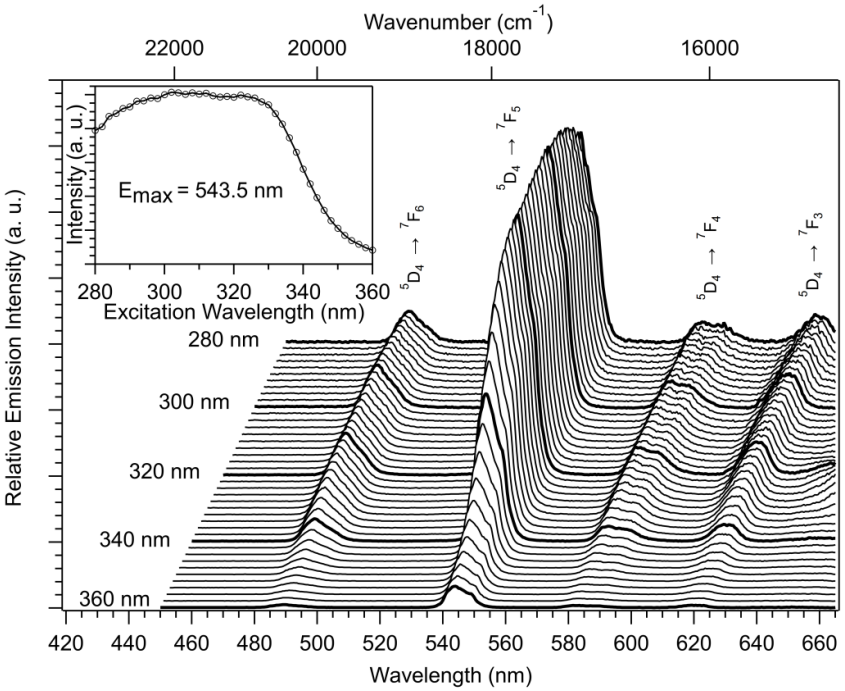

Figure S5: Emission spectra versus excitation wavelength (280 – 360 nm) at 293 K on a single-crystal of **Tb-TEMPO-CN**. Inset: maximum intensities versus excitation wavelength of the $^5D_4 \rightarrow {}^7F_5$ transition from Tb(III) at 543.5 nm.

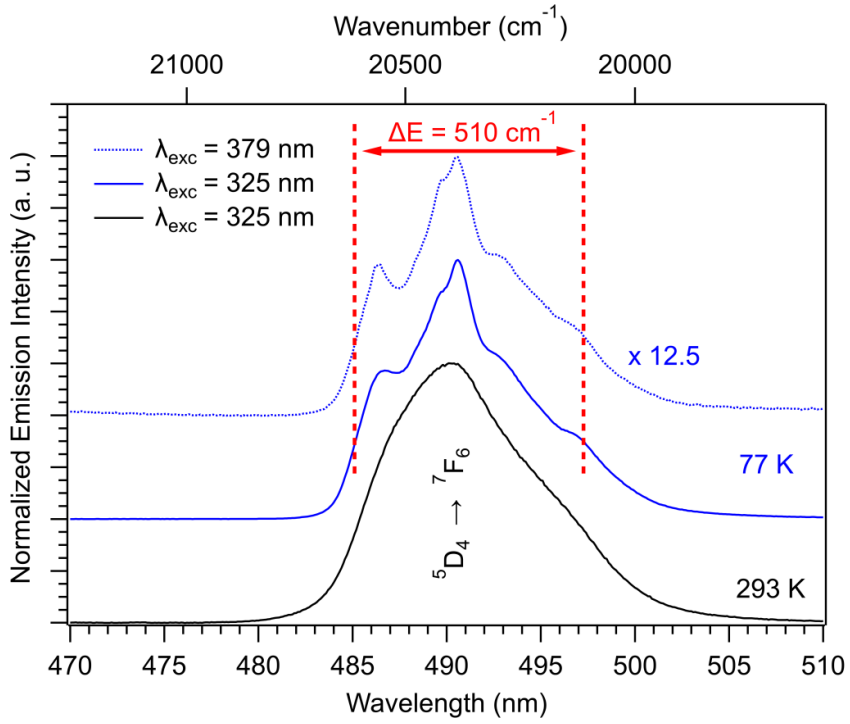

Figure S6: Emission spectra on a single-crystal of **Tb-TEMPO-CN** at 293 K (dark curve) and 77 K (blue curves). λ_{exc} = 325 nm (absorption from the ligand) and 379 nm (absorption from the lanthanide). The emission upon photo-excitation at 379 nm is multiplied by 12.5.

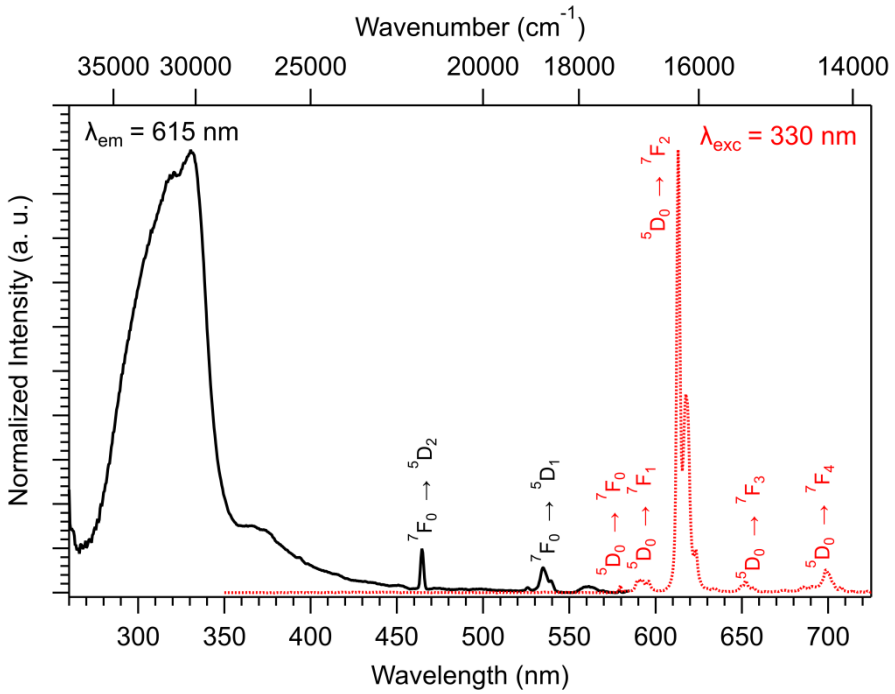

Figure S7: Excitation (dark curve, λ_{em} = 615 nm) and emission (red dotted curve, λ_{exc} = 330 nm) spectra on a powder of **Eu-TEMPO-CN** at 293 K.

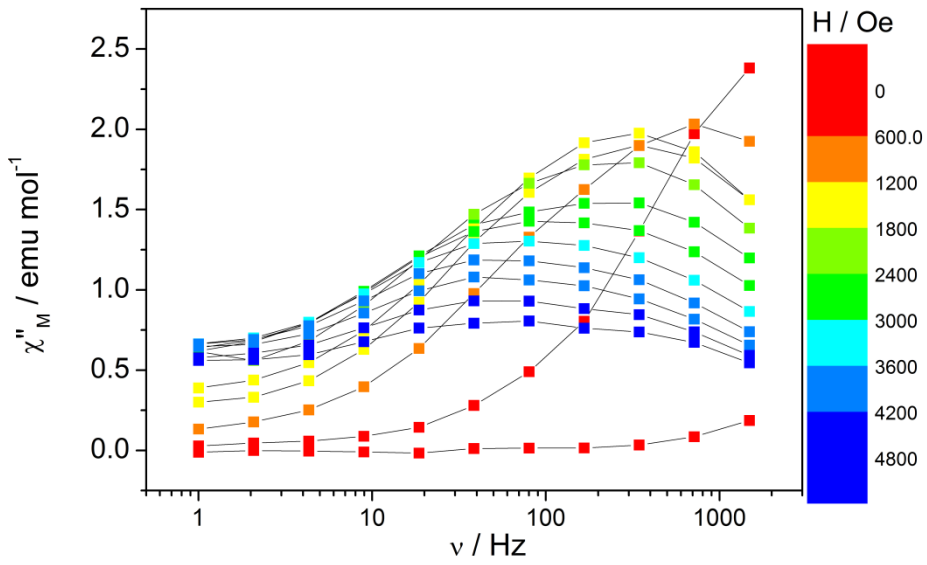

Figure S8. Frequency dependence of the out-of-phase magnetic susceptibility of **Dy-TEMPO-CN** (T = 2 K) for various static magnetic fields.

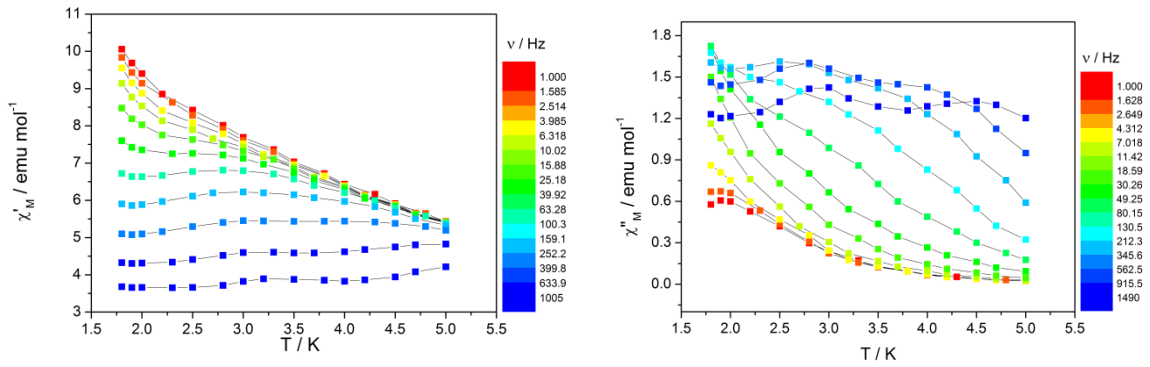

Figure S9. Temperature dependence of the in-phase (left) and out-of-phase (right) magnetic susceptibility of **Dy-TEMPO-CN** (Hdc = 2400 Oe). Lines are guides to the eye.

Table S4. Values extracted from the fitting of χ_M'' vs frequency curves of **Dy-TEMPO-CN** (H_{dc} = 2400 Oe).

T (K)	τ (μs)	T (K)	τ (μs)
1.8	1672.61	3.25	270.34
1.9	1269.84	3.5	262.23
2	875.38	3.75	242.63
2.25	544.39	4	206.75
2.5	383.36	4.25	175.21
2.75	307.26	4.5	141.99
3	278.09		

Table S5. Values extracted from the Cole-Cole plot of **Dy-TEMPO-CN** (H_{dc} = 2400 Oe).

T (K)	χ_S	χ_T	α	R^2
1.8	1.94319	10.74131	0.51179	0.9776
1.9	1.67131	10.41287	0.54124	0.98668
2	1.4045	10.12312	0.55793	0.98683
2.25	1.01796	9.39797	0.56181	0.96987
2.5	1.01086	8.74733	0.51877	0.96286
2.75	1.32187	8.1649	0.44802	0.97983
3	1.72343	7.76307	0.39074	0.97979
3.25	2.23199	7.38398	0.32443	0.98082
3.5	2.49995	7.03281	0.2665	0.98404
3.75	2.84457	6.65394	0.16425	0.97569
4	2.53945	6.42348	0.19555	0.98616
4.25	2.42863	6.15	0.18383	0.98468
4.5	2.34907	5.89827	0.16669	0.98759

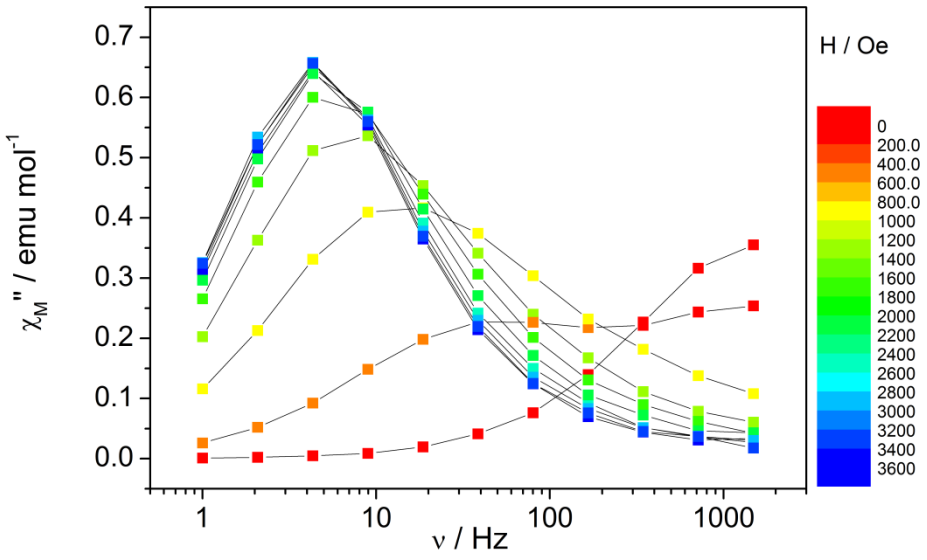

Figure S10: Frequency dependence of the out-of-phase magnetic susceptibility of **Tb-TEMPO-CN** (T = 4 K) for various static magnetic fields.

Table S6. Values extracted from the fitting of χ_M'' vs frequency curves of **Tb-TEMPO-CN** (H_{dc} = 2000 Oe).

T (K)	τ (μs)	T (K)	τ (μs)
3.2	100512.2	6.6	2334.4
3.4	69606.7	6.8	1958.8
3.6	50727.9	7	1666.7
3.8	37960.8	7.2	1402
4	29618.1	7.4	1197
4.2	22846.7	7.6	966.7
4.4	18195.8	7.8	842.6
4.6	14728.1	8	706.6
4.8	11787.1	8.2	589
5	9676.4	8.4	490.8
5.2	7962.6	8.6	414.2
5.4	6585.4	8.8	345.7
5.6	5483.1	9	292.5
5.8	4583.5	9.2	248.2
6	3851.4	9.4	210.8
6.2	3254.7	9.6	177.8
6.4	2741.2	9.8	150.8

Table S7. Values extracted from the Cole-Cole plot of **Tb-TEMPO-CN** (H_{dc} = 2000 Oe).

T (K)	χ_S	χ_T	α	R^2
2	0.36148	3.61205	0.44133	0.99841
3	0.30059	2.94347	0.39575	0.999
4	0.26492	1.97194	0.20997	0.98741
5	0.22804	1.54456	0.10952	0.98476
6	0.1968	1.29024	0.05868	0.99128
7	0.17513	1.11593	0.0396	0.99582
8	0.16315	0.98424	0.01743	0.99503
9	0.15747	0.87827	0.00532	0.98851

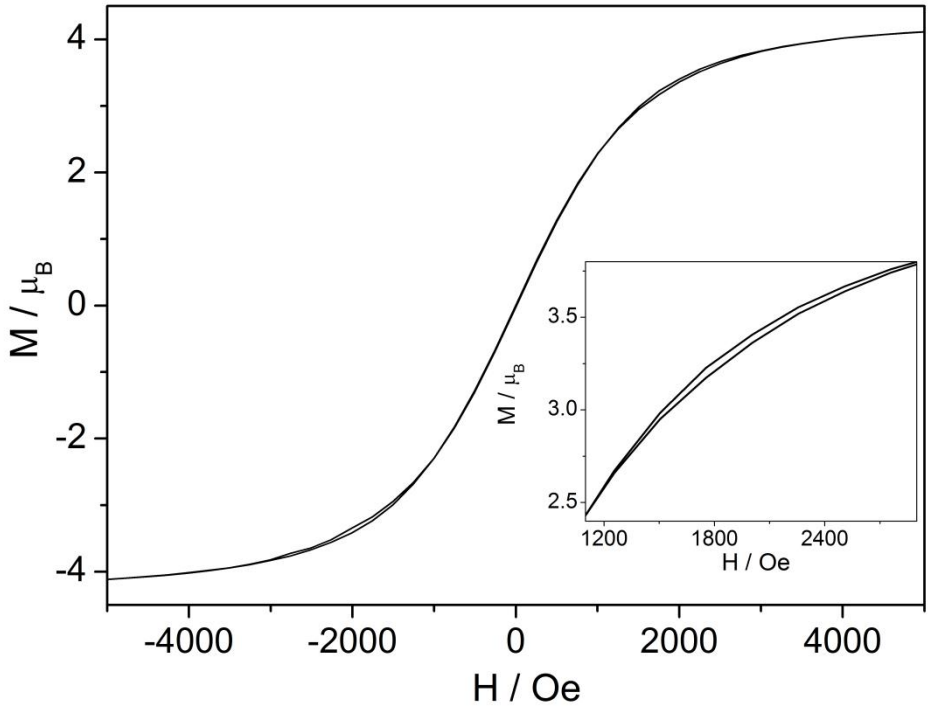

Figure S11. Hysteresis loop for **Tb-TEMPO-CN** measured at 0.5 K with a magnetic field sweep rate of 16 Oe.s^{-1}.

Ab initio calculations

Table S8: Computed CASSCF/RASSI-SO energy levels (in cm^{-1}) of Tb^{III} ion in **Tb-TEMPO-CN**.

1	0.000	21	2370.636	41	5335.953
2	0.174	22	2379.120	42	5444.886
3	149.443	23	2488.102	43	5456.443
4	153.136	24	2497.925	44	5585.223
5	220.548	25	3538.634	45	5593.283
6	226.896	26	3593.711	46	5860.146
7	239.804	27	3624.713	47	6000.947
8	264.382	28	3659.537	48	6109.922
9	288.160	29	3678.101	49	6252.075
10	358.517	30	3717.200		
11	366.634	31	3757.949		
12	499.925	32	3806.031		
13	500.745	33	3867.520		
14	2163.371	34	4626.973		
15	2167.372	35	4681.979		
16	2246.797	36	4701.497		
17	2266.788	37	4725.474		
18	2309.845	38	4733.013		
19	2323.336	39	4781.401		
20	2336.274	40	4786.983		

(1) Alvarez, S. Polyhedra in (inorganic) chemistry. *Dalton Trans.* **2005**, 2209-2233.